nature biomedical engineering

PERSPECTIVE

https://doi.org/10.1038/s41551-020-00681-x

Harnessing non-destructive 3D pathology

Jonathan T. C. Liu[1,2,3]✉, Adam K. Glaser[1], Kaustav Bera[4], Lawrence D. True[2], Nicholas P. Reder[1,2], Kevin W. Eliceiri[5,6,7]✉ and Anant Madabhushi[4,8]✉

High-throughput methods for slide-free three-dimensional (3D) pathological analyses of whole biopsies and surgical specimens offer the promise of modernizing traditional histology workflows and delivering improvements in diagnostic performance. Advanced optical methods now enable the interrogation of orders of magnitude more tissue than previously possible, where volumetric imaging allows for enhanced quantitative analyses of cell distributions and tissue structures that are prognostic and predictive. Non-destructive imaging processes can simplify laboratory workflows, potentially reducing costs, and can ensure that samples are available for subsequent molecular assays. However, the large size of the feature-rich datasets that they generate poses challenges for data management and computer-aided analysis. In this Perspective, we provide an overview of the imaging technologies that enable 3D pathology, and the computational tools—machine learning, in particular—for image processing and interpretation. We also discuss the integration of various other diagnostic modalities with 3D pathology, along with the challenges and opportunities for clinical adoption and regulatory approval.

Disease diagnosis often depends on the rapid and accurate pathological analysis of biopsied and surgically excised tissues. The careful interrogation of the morphological and molecular characteristics of biopsied tissue helps to determine the grade of the disease. For many cancers, this information then provides the basis for stratifying patients for clinical management, and can result in markedly different treatment paths[1,2]. For example, patients with low-grade prostate cancer (Gleason score below 7) are candidates for active surveillance, and patients with a Gleason score of 7 and above are candidates for curative therapy (radiation and/or surgery), often in conjunction with neoadjuvant therapy for those with the highest-grade cancer (Gleason scores 8 to 10). Interobserver variance among pathologists can however be high, with Cohen's kappa values[3–6] ranging from 0.3 to 0.8 (Cohen's kappa values are a measure of the agreement between individual results, with values lower than 0.2 indicating poor agreement and values between 0.8 and 1.0 indicating very good agreement). This contributes to the overtreatment of certain patients with indolent disease[7,8], resulting in unnecessary side effects and in financial toxicity to patients and the healthcare system. Likewise, the undertreatment or the non-optimal treatment of patients with aggressive and late-stage disease leads to preventable morbidity and mortality[9], along with substantially increased costs of care.

Treatments for patients with non-small-cell lung cancers are another example of the shortcomings and opportunities for anatomic pathology. For these patients, the use of immune-checkpoint inhibitors against the programmed cell death protein 1 (PD-1) or its ligand (PD-L1) can decrease the risk of progression by up to 60% (compared with standard chemotherapy); yet these drugs are only effective in approximately 20% of the patients[10]. With treatment costs ranging from US$150,000 to US$1 million per patient for a full course of treatment, as well as the possibility of autoimmune side effects, reliable assays are needed to identify the patients most likely to respond to these treatments. Current companion and complementary diagnostic tests for predicting responses to PD-1 and PD-L1 inhibitors are based on immunohistochemical analysis of PD-L1 expression, but these methods have been criticized for their unreliability[11,12]. The shortcomings of these assays are typically attributed to the variability in interpretation of PD-L1 immunohistochemistry data[13] by the pathologist, the spatial and temporal heterogeneity of PD-L1 expression within the tumour microenvironment, and the general complexity of the immune response in which a durable immunomodulatory response involves the coordinated interaction of multiple cell types.

Pathology laboratories currently handle biopsies and surgical specimens following a decades-old analogue imaging workflow that samples only a small fraction of each specimen. The reliability of pathological tests therefore suffers because the undersampling of a heterogeneous tissue specimen is bound to introduce errors. For example, a standard 5-μm-thick section of a 1-mm-thick biopsy represents only 0.5% of the biopsy. Moreover, the workflow of traditional slide-based pathology is time consuming and inherently destructive, making it incompatible with modern-era molecular medicine, in which increasing numbers of assays (for example, genomics and proteomics assays), which rely on having abundant tissue[14], are desired for personalized care. In addition to sampling limitations, the thin-slide-mounted tissue sections that are typically viewed by pathologists provide only a 2D view of tissue structures and molecular targets, which can be challenging to interpret accurately and reproducibly[15–17]. Digital pathology, in combination with objective machine-learning-based analysis methods, strives to improve the reproducibility and reliability of diagnostic pathology[18].

Technological advances in optical clearing, high-throughput microscopy and computational tools, including artificial intelligence (AI), have fuelled interest in non-destructive 3D pathology as a complement to traditional slide-based 2D pathology, on the grounds that non-destructive volumetric microscopy can improve the accuracy (diagnostic, prognostic and predictive power) of the analysis of tissue specimens, resulting in superior patient outcomes. The benefits of 3D pathology over traditional pathology include:

[1]Department of Mechanical Engineering, University of Washington, Seattle, WA, USA. [2]Department of Laboratory Medicine and Pathology, University of Washington, Seattle, WA, USA. [3]Department of Bioengineering, University of Washington, Seattle, WA, USA. [4]Department of Biomedical Engineering, Case Western Reserve University, Cleveland, OH, USA. [5]Department of Medical Physics, University of Wisconsin, Madison, WI, USA. [6]Department of Biomedical Engineering, University of Wisconsin, Madison, WI, USA. [7]Morgridge Institute for Research, Madison, WI, USA. [8]Louis Stokes Cleveland Veterans Administration Medical Center, Cleveland, OH, USA. ✉e-mail: jonliu@uw.edu; eliceiri@wisc.edu; anant.madabhushi@case.edu

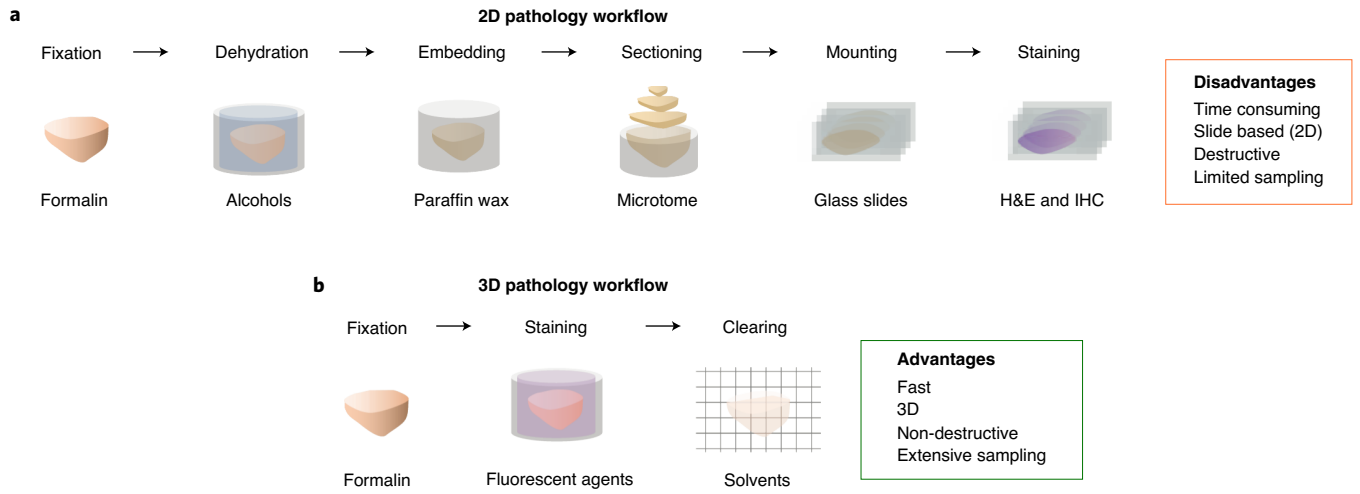

Fig. 1 | Conventional pathology versus non-destructive 3D pathology. a, The conventional histology workflow was developed over a century ago and involves the use of harsh fixatives and dehydration reagents (such as xylene) followed by wax embedding, destructive sectioning and the staining of slide-mounted sections with chromogens, such as H&E, or for immunohistochemistry (IHC). In addition to being time consuming and destructive, conventional 2D imaging allows the viewing of only a small fraction of the clinical specimen. **b**, Advances in optical clearing and fluorescent labelling, along with high-throughput volumetric microscopy, have enabled entire specimens (for instance, core-needle biopsies) to be imaged in three dimensions, with minimal requirements for tissue processing and mounting. 3D pathology provides rich structural and molecular information from large intact specimens, and preserves valuable clinical specimens for downstream assays (such as DNA and RNA sequencing).

improved sampling of large volumes of tissue rather than sparse sampling with slide-mounted sections; volumetric imaging of diagnostically relevant structures; non-destructive imaging, which allows intact tissue specimens (such as core-needle biopsies) to be made fully available for downstream proteomic and genetic assays; and a simpler slide-free imaging process, which could save time and costs (Fig. 1).

Although the full value of data from 3D pathology has yet to be determined, three illustrative examples help to contextualize the expected gains (Fig. 2). First, 3D pathology accurately shows convoluted structures, such as branching-tree vascular and glandular networks. Such structures are often disrupted during disease progression and can be predictive of patient prognosis and treatment responses. When viewing such complex 3D structures as 2D cross-sections on glass slides, artefacts and ambiguities are unavoidable. This is particularly problematic for the Gleason grading of prostate cancers, which is currently based solely on glandular architecture. For example, what appears in two dimensions to be a poorly formed gland (a variant of Gleason pattern 4) might be a tangential section of a well-formed gland (Gleason pattern 3). Consequently, such a cancer could be re-categorized from the 2D-determined grade (Gleason score 3+4=7) to a lower-grade Gleason score (3+3=6) when viewed in three dimensions (which could result in markedly different treatment recommendations)[19,20]. Second, 3D pathology can better characterize and quantify the spatial relationships and interactions between cell types. This is exemplified by the complex distributions of cells within the tumour immune microenvironment, such as the extent and proximity of PD-1-expressing cytotoxic T cells to PD-L1-expressing cancer cells[21], and the balance of immunosuppressive neutrophils and cytotoxic T cells[22,23]. The ability to interrogate larger volumes of tissue would be beneficial, as spatial heterogeneity is a characteristic of most diseases when viewed at microscopic length scales[24–26]. Third, 3D pathology can identify rare cells that may have a critical role in the initiation, dissemination and resistance to treatment of various diseases. Examples of rare cells that are difficult to identify in thin tissue sections include tumour progenitor cells[27–29], minimal residual disease following treatment[30,31], and aggressive tumour subclones that invade the lymphovascular network[32–34] and metastasize[35]. It is increasingly clear that complex distributions of rare cell populations, such as cancer stem cells, have pivotal roles in many aspects of oncology[36–38]. This understanding of tumours as hierarchical collections of cells with substantial intratumoral heterogeneity is still being refined.

The current status of 3D pathology

The concept of 3D pathology is not new, yet the technologies have evolved considerably over the years. Early studies relied on destructive serial-sectioning techniques[39], which required considerable expense and labour for imaging large numbers of sectioned tissues and for subsequent 3D reconstruction. Automated serial-sectioning approaches, such as knife-edge scanning and micro-optical-sectioning tomography[40,41], have greatly improved throughput and have been commercialized for the purposes of delivering 3D pathology data, but are destructive of tissue specimens and introduce sectioning artefacts (Fig. 3a).

Non-destructive 3D microscopy has been embraced (and been largely driven) by life scientists, and has been catalysed primarily by developments in confocal microscopy, followed by multiphoton microscopy and, most recently, by light-sheet microscopy (Fig. 3a,b). In clinical diagnostics, however, 3D pathology is in its infancy. This is mostly because of barriers for the technical adoption of advanced microscopy devices, tissue-preparation techniques and computational analysis methods. Increasing numbers of research groups are now exploring diagnostic applications of 3D pathology. Below we provide a non-exhaustive survey of studies that have used 3D pathology.

With optical clearing of archival formalin-fixed paraffin-embedded (FFPE) and fresh prostate tissues, confocal microscopy has been shown to be a feasible imaging method for clinical diagnostics[42]. Similarly, multiphoton microscopy with optical clearing has been used to generate 3D histology images of kidney biopsies[15]. Light-sheet microscopy has recently been used to examine optically cleared FFPE specimens (from bladders), showing the ability to quantify certain histomorphometric features, such as vascular density and tortuosity[43], and to analyse the lymphatics within bladder tumours[44], suggesting that 3D pathology is superior to 2D

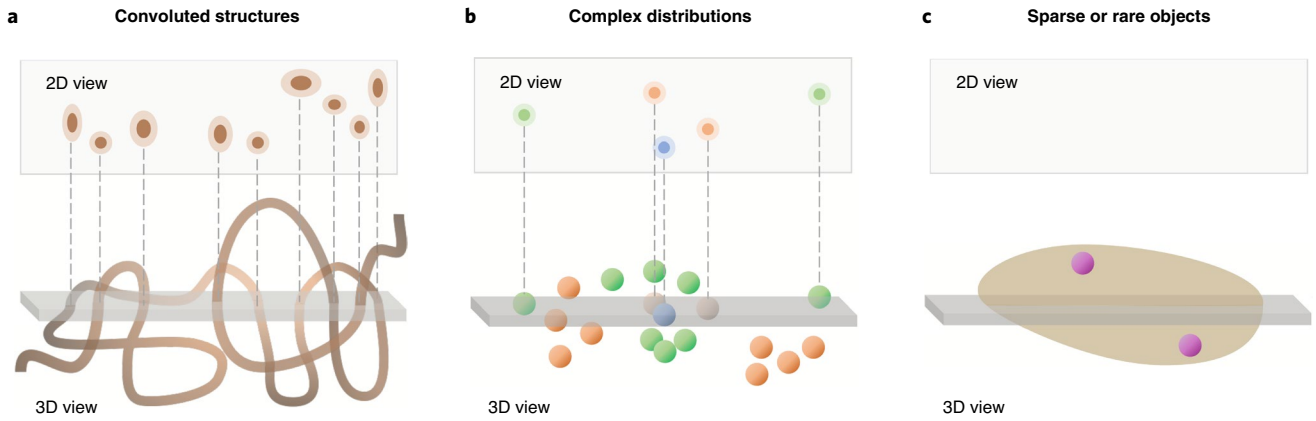

Fig. 2 | 3D pathology can outperform 2D pathology. a, For convoluted 3D structures, such as prostate glands, tumour vasculature and kidney tubules, 2D cross-sectional views can be misleading. **b**, For distributions of cells and other structures, 2D cross-sectional views might preclude the accurate quantification of complex spatial relationships, such as those found within the tumour immune microenvironment and the cancer stem cell niche. **c**, For rare objects, such as tumour-initiating cells, lymphovascular invasion and minimal residual disease, 2D sections might not provide adequate sampling to identify and quantify such targets.

pathology for staging cancers and for predicting progression-free survival. Studies using an open-top light-sheet (OTLS) microscopy system, specifically designed for high-throughput imaging of large clinical specimens, indicated that 3D pathology could improve the grading of prostate core-needle biopsies by mitigating some of the ambiguities and artefacts encountered when viewing 2D tissue sections of prostate carcinoma[19]. A follow-up study used the OTLS technology[20] to show that high variability in glandular morphology throughout an entire core-needle biopsy could have a marked influence on treatment decisions, providing additional insight into the potential clinical value of 3D pathology. More recently, 3D confocal microscopy of immune infiltrates in preclinical and human core-needle biopsies (from head and neck cancer) revealed that the spatial distribution of tumour-infiltrating cytotoxic T cells is correlated with other hallmarks of disease progression, such as the extent of the tumour microvasculature[45]. In addition, a detailed investigation of the 3D structure of prostate cancers revealed two major architectural subgroups of growth patterns that could be of prognostic value[46]. Note that this Perspective does not discuss the rapid ex vivo[19,47–56] and in vivo[57–61] examinations of tissues and wound cavities to guide surgical decisions, despite some overlap in technologies.

Radiomics—the quantitative interrogation and subsequent mining of pixel-level sub-visual data from standard medical imaging methods, such as ultrasound, computed tomography (CT), positron emission tomography (PET) or magnetic resonance imaging (MRI)—is a non-invasive image-analysis method that can answer clinically relevant questions pertaining to diagnosis, prognosis and treatment response across the oncology spectrum[62,63]. Radiomics has traditionally relied on analysing multiple 2D images across a region of interest, with interpolation being used to extend the analysis to three dimensions. 3D pathology resembles radiomics, but differs in a few key aspects. Unlike a conventional CT slice, with dimensions of 512 × 512 pixels, a whole-slide image at 20× magnification is often 40,000 × 40,000 pixels in size; that is, 4 orders of magnitude larger. This introduces challenges in big-data handling, but also opportunities for developing AI approaches that thrive on large and diverse training datasets. In addition, unlike reconstructed radiographic images, 3D pathology images contain large numbers of highly repetitive microscale features (primitives), such as cells, nuclei, glands and stromal structures, which can aid the efficient training and use of AI methods.

Technologies for non-destructive 3D pathology

In this section, we overview protocols for tissue clearing and labelling, imaging modalities and technical imaging requirements, as well as computational methods for data processing and for the visualization and analysis of the images.

Protocols for tissue clearing and labelling. Numerous protocols have been developed to improve the transparency of excised biological tissues for the purposes of enabling deep optical imaging at high resolution[64,65]. Optical clearing seeks to homogenize the refractive index profile within tissues, primarily through replacement of the water within the tissue (refractive index approximately 1.33) with a high-refractive-index solvent that is better matched to the remaining tissue components (mostly proteins and lipids). Certain protocols also perform lipid removal with detergents, in some cases accelerated by active electrophoretic transport, and even decalcification to enable optical imaging through bone[66,67]. Early protocols were developed for the clarification of brain tissue for neuroscience applications, with limited optimization for other organs[68–71]. Such protocols were often complex, including the use of hydrogel embedding to preserve the structure of delicate brain tissues and maintain the brightness of genetically encoded fluorescent proteins[70,72,73]. Recent efforts have focused on clearing whole organisms and various types of human tissue[66,67,74,75]. A relatively simple method that has gained popularity for clearing a variety of preclinical and clinical tissues is iDISCO[74], and a more recent variant that uses a food-grade cinnamon oil[75] (ethyl cinnamate) for final index matching rather than the dibenzyl ether used in the original protocol, which is corrosive and carcinogenic. Note that different clearing protocols exhibit varying levels of compatibility with fluorescent labelling approaches, including small-molecule fluorescent probes and large antibodies[64,76]. Small-molecule probes that mimic standard histology stains, such as haematoxylin and eosin[19,77,78] (H&E) and periodic acid Schiff[79] staining, have the advantage of being inexpensive (relative to antibodies), of diffusing quickly within thick 3D specimens, and of being compatible with a variety of clearing techniques. Such small-molecule probes will therefore probably have a prominent role in early clinical assays based on 3D pathology.

For clinical applications of 3D pathology, unique requirements and constraints exist for tissue processing in preparation for imaging. First and foremost, until these techniques become the standard of care, they should ideally not interfere with current histopathology

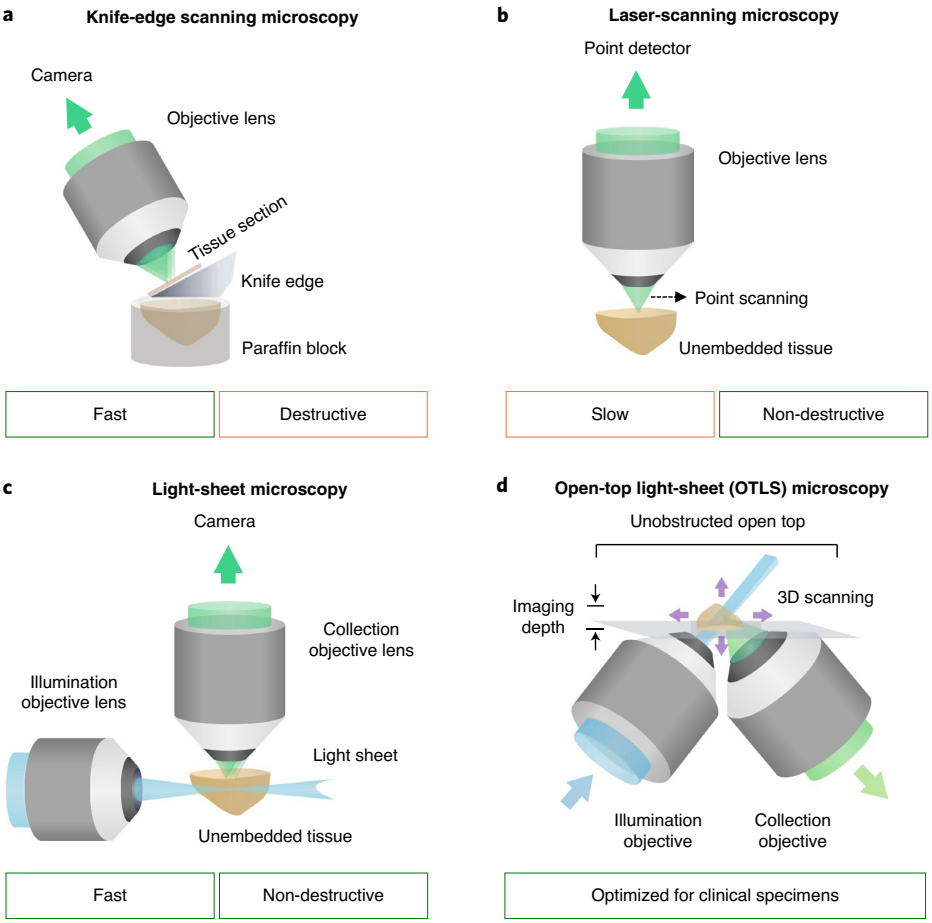

Fig. 3 | Selected imaging methods for 3D pathology. a, Knife-edge scanning microscopy and micro-optical-sectioning tomography are destructive methods in which 2D images are acquired as a specimen is serially sectioned. The stacks of adjacent 2D images are used to reconstruct a 3D image of the specimen. **b**, With confocal microscopy and multiphoton laser-scanning microscopy, a single point is typically illuminated within a thick specimen, and is spatially scanned in three directions to non-destructively generate a 3D image over time. **c**, With light-sheet microscopy, a 2D optical section within a transparent thick specimen is illuminated. Fluorescence generated within that light sheet is imaged in the orthogonal direction onto a sensitive high-speed camera. Scanning the 2D light sheet through the sample (or vice versa) allows for the rapid generation of a 3D image plane by plane. **d**, The architecture of an OTLS microscope allows for laterally unconstrained imaging of one or more specimens placed on a transparent sample holder (similar to a flat-bed scanner for tissues). Angled light-sheet images, extending into the specimen, are rapidly collected by a camera (via the collection objective) as the specimen is moved. To image large tissue volumes, the sample holder is translated laterally and vertically.

methods, such as slide-based H&E staining and immunohistochemistry. For most clearing methods, the reagents are relatively gentle compared with formalin fixation. In other words, once the tissue is fixed in formalin—as is currently required within strict timeframes following clinical biopsy or tissue resection—subsequent steps for most 3D pathology pipelines are less harsh and damaging to the tissue and to its molecular constituents (proteins, DNA and RNA). Nonetheless, rigorous demonstration of the compatibility of 3D pathology methods with standard pathology techniques is necessary. Initial studies have shown that fixed and deparaffinized tissues that are labelled with fluorescent stains and cleared using iDISCO, ethyl cinnamate or similar protocols can be subsequently embedded in paraffin and subjected to standard H&E and immunohistochemistry methods with no apparent degradation in quality[20,43,56].

3D pathology could also introduce new tissue-preservation methods. In particular, as genomics and transcriptomics assays rapidly improve and gain clinical acceptance, a major performance bottleneck is the damaging effects that formalin fixation has on the integrity of DNA and RNA. Alternative tissue-preservation methods, such as RNAlater[80,81] and PAXgene[82,83], have been developed to maintain the fidelity of nucleic acids. Furthermore, a tissue-preservation protocol that relies on the intramolecular and intermolecular crosslinking of biomolecules has enabled the effective optical clearing and fluorescent labelling of molecular targets, including RNA transcripts[84]. The ability to incorporate and standardize new tissue-preservation strategies within a clinical pipeline for 3D pathology that are capable of high-quality volumetric imaging and sensitive nucleic acid detection could be transformational for precision medicine.

Technical imaging requirements for 3D pathology. Although there are many factors to consider when designing any 3D optical imaging system, key attributes include its resolution, contrast (signal-to-background ratio), speed or throughput, ease of use and cost. Among them, ease of use and speed or throughput are of higher priority in anatomic pathology (rather than in scientific research) because pathologists generally do not image tissues at the highest levels of resolution used for basic biological studies (for example, with high-numerical-aperture (NA) oil-immersion objectives (NA > 1.0)). With the exception of a few specialties such as renal pathology, which routinely uses electron microscopy, the vast majority of anatomic pathology cases are viewed at low

resolution (using standard 5× to 10× objectives with NAs of 0.1–0.3) and occasionally at moderate resolution (using standard 20× to 40× objectives with NAs of 0.4–0.8). Rather, in light of the spatial and molecular heterogeneity of neoplastic lesions[26,85], the ability to view large areas or volumes of tissue is often of paramount importance for pathologists.

Image contrast is important because it directly impacts imaging depth. Although biologists rely on optical-sectioning microscopes to image living organisms and tissues at reasonable depths (up to about 0.5 mm for confocal and multiphoton microscopy in certain optically scattering tissues), pathologists tend to examine excised and preserved specimens, where recent advances in optical clearing enable such excised tissues (including bone) to be rendered highly transparent[65,71,72,74,86–88]. In short, for 3D microscopy techniques, optical clearing now allows tissues to be imaged at depths of several millimetres and even centimetres, while greatly relaxing the requirements for contrast (rejection or suppression of background light).

Confocal and multiphoton laser-scanning microscopy. The traditional workhorse technologies for the non-destructive high-resolution 3D imaging of tissues have been confocal microscopy, and nonlinear or multiphoton microscopy[49,50,89–91]. Confocal microscopy[42,46,92] is the most prevalent volumetric microscopy technique in academic and industrial laboratories. Multiphoton microscopy has also been widely adopted in academic research, owing to its ability to provide enhanced imaging depths (contrast) when imaging turbid (uncleared) tissues, and also because it can achieve label-free imaging by relying on a number of linear and nonlinear contrast mechanisms, such as autofluorescence generation[50,54,90,93–96], second-harmonic generation[97–99], coherent four-wave mixing[51,52,90,100,101] (such as coherent anti-Stokes Raman spectroscopy and stimulated Raman scattering), and pump–probe methods[102,103]. Multiphoton microscopy has been recently employed in clinical applications of anatomic pathology, such as surgical guidance and diagnosis[15,50,90,96,104].

Because they offer exquisite contrast (that is, rejection of background) and spatial resolution, confocal and multiphoton microscopy have become ubiquitous in biomedical research laboratories. For clinical applications, however, these techniques need to overcome a number of challenges. In particular, confocal microscopy and nonlinear microscopy typically generate an image in a point-by-point fashion, which requires spatial scanning in all three dimensions to create a volumetric image (Fig. 3b). This tends to add mechanical complexity, and is often slow. Although there are methods to accelerate this process, such as the use of spinning discs for confocal microscopy[105,106], and of temporal focusing[107,108] or multifocal methods[109–111] for nonlinear microscopy, speed is often still a major constraint when trying to image large volumes. Furthermore, these technologies rely on complex high-NA optics, high-speed laser scanning and pulsed lasers (for multiphoton microscopy), and are thus expensive in terms of equipment and technical support staff.

Light-sheet microscopy for 3D pathology. Light-sheet microscopy, also known as selective plane illumination microscopy, enables rapid 3D fluorescence microscopy of relatively transparent specimens (such as embryos and optically cleared tissues)[112–120]. This technique makes use of a thin excitation plane of light that enters the tissue and excites a fluorescence signal from a localized plane (or optical section) within the sample. This thin plane or sheet of fluorescence signal is then imaged along a detection axis oriented roughly perpendicular to the light sheet (Fig. 3c). Light-sheet systems use highly sensitive and fast scientific complementary metal–oxide–semiconductor (sCMOS) detector arrays to obtain 2D images from a specimen, from which a 3D dataset may be rapidly generated by moving the specimen in relation to the light sheet. In addition to the speed of imaging that light-sheet microscopy enables, which is essential for clinical applications, another well-appreciated feature of light-sheet microscopy is its highly efficient geometry: it excites fluorescence only within the detection plane, thereby minimizing photobleaching and photodamage when compared with alternative 3D microscopy techniques[114,115,117]. Hence, light-sheet microscopy has been referred to as a 'gentle' form of 3D microscopy[121].

Early light-sheet microscopes were constrained to image small non-clinical specimens (such as embryos and mouse brains) that were often embedded in agarose or put on specialized mounts (for sample rotation, in particular), thus limiting the size and geometry of the specimens and the systems' ease of use[115,117,120,122]. More recently, a number of light-sheet microscope systems have been developed to accommodate larger specimens with fewer physical constraints and simpler mounting requirements[19,77,118,120,123–132]. Many of these systems use an inverted architecture, in which one or more tissue samples may be conveniently placed on a platform and imaged from above or from below. In particular, imaging from below the specimens is the basis of OTLS microscopy (Fig. 3d), which has been shown to be a convenient configuration for imaging one or more large clinical specimens[19,77,127,132,133].

OTLS microscopes—which are configured like flat-bed scanners for tissues—are ideal for the convenient mounting and imaging of clinical specimens of diverse geometries and numbers (through multisample holders and well plates)[19,20,56,77,134]. OTLS systems also provide unconstrained space above the sample, offering the potential to incorporate tissue-manipulation accessories—such as fluid-exchange systems, dissection and aspiration devices, and robotic sample exchangers—for streamlining 3D pathology for clinical applications. One challenge for OTLS (and for other forms of inverted light-sheet microscopy) is that the imaging depth can be limited if the imaging objectives are oriented at an oblique angle with respect to a horizontal sample holder, as this prevents the full working distance of the objectives from being usable for imaging within the specimen (Fig. 3d). The working distance of an objective must typically trade-off with its NA, a parameter that is proportional to the cone angle of focusing and that dictates the level of spatial resolution that can be achieved (a larger NA allows smaller features to be resolved). Therefore, for inverted light-sheet microscopes that are designed to image specimens at depths of several millimetres, resolution is often limited to the low-to-moderate range (>0.4 μm with an objective with NA < 0.8). This level of resolution is optimal for the vast majority of clinical diagnostic applications, where imaging larger volumes of tissue in a timely manner is often the top priority for achieving accurate diagnostic determinations. To maximize imaging depth and resolution, one can use a single high-NA objective oriented perpendicular to the sample to generate both an oblique-illumination light sheet and to image the light-sheet-generated fluorescence signal onto a detector array (camera)[130–132,135–137,138]. This strategy of using a single objective for light-sheet microscopy, while convenient, introduces certain constraints and trade-offs[139], which has motivated additional innovations, including multiresolution systems that mimic the ability of conventional pathology microscopes to image tissues at various magnifications[140,141].

Data handling challenges. For all 3D microscopy techniques, the digital reconstruction of large 3D images requires the stitching and fusing of large numbers of 2D image tiles. Once generated, the sizes of these 3D datasets can easily reach terabyte scales (depending on sample size and spatial resolution). This brings about challenges in data storage, low-loss compression, quality control and visualization. In order to streamline the management of increasingly large amounts of data, standard open source informatics tools and annotated datasets should be established. 3D microscopy generates vastly more data compared with conventional 2D microscopy approaches (Fig. 4). However, data generation speeds (about 800 MB s^{-1}) are

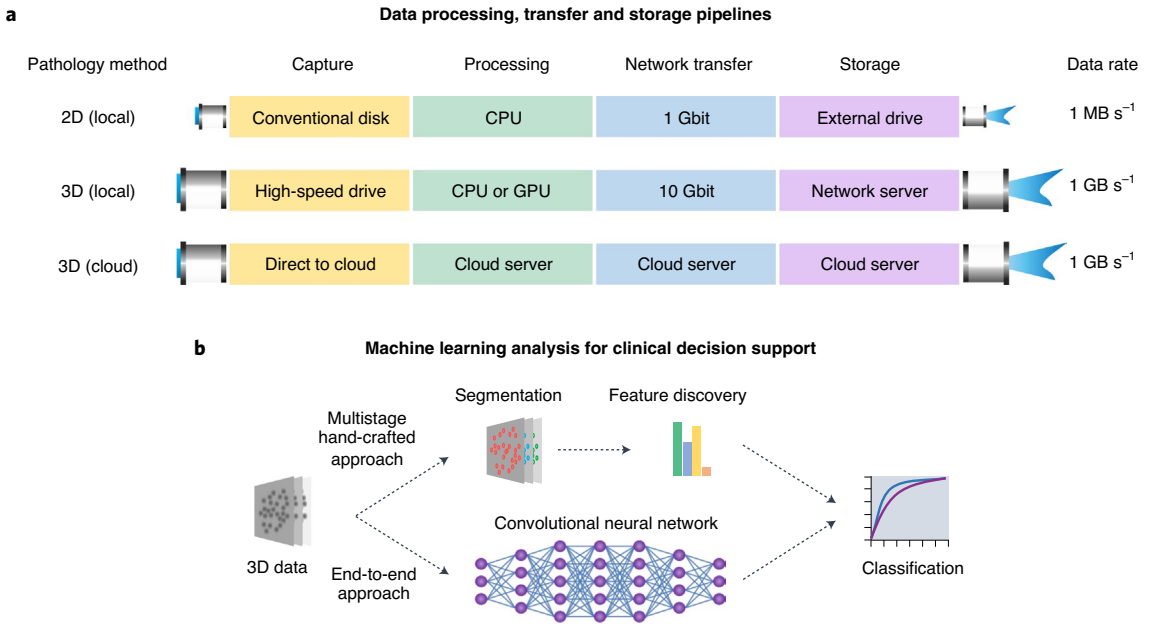

Fig. 4 | Data processing and image-analysis workflows. a, Light-sheet microscopes acquire data at up to 1 GB s^{-1} and require specialized hardware, such as a local 10 Gbit networked server, or a cloud-based storage and analysis solution. **b**, Machine learning tools will be necessary to assist with the analysis of large 3D pathology datasets for clinical decision support. Strategies include end-to-end deep learning models that directly classify the raw images, as well as multistage approaches that first segment well-understood microstructures, from which hand-crafted features are extracted and used as inputs for prognostic and predictive classifiers. Multistage hand-crafted approaches can incorporate deep learning techniques to, for example, assist with segmentation tasks. CPU, central processing unit; GPU, graphics processing unit. Note that for the segmentation and feature discovery steps within a multistage approach, both traditional or deep learning methods can be used.

similar to those of current whole-slide imaging (WSI) devices that use similar sCMOS camera technologies; this should facilitate the adoption of 3D datasets by institutions that are already accommodating a digital pathology workflow. Further, the standardization of image formats (such as digital imaging and communications in medicine (DICOM)) between commercial platforms should facilitate data sharing and clinical adoption. Figure 4 outlines various strategies for processing raw data from 3D microscope systems (for instance, local versus cloud-based pipelines), as well as general strategies for the machine-learning-based analysis of these massive feature-rich datasets.

Image stitching. A key step in the acquisition pipeline for 3D microscopy data is the efficient assembly of large numbers of 2D image tiles into seamless volumetric datasets. A number of commercial software packages (such as Imaris Stitcher and Volocity) as well as popular open source tools (such as TeraStitcher[142,143] and BigStitcher[144]) have been developed to address this challenge. Some software tools (in particular, BigStitcher) are designed to correct for deformation and registration artefacts through affine transformations, including chromatic shifts between wavelength channels. Such operations can be computationally expensive, and should ideally be tailored to specific imaging methods and parallelized for maximum throughput (for example, open source efforts are improving the popular hierarchical multiresolution HDF5 file format with a similar format, N5, which will allow for parallel writing (https://github.com/saalfeldlab/n5)). For the clinical implementation of 3D pathology, quality control algorithms will ultimately be needed to ensure the performance of these and other image-processing tasks.

Compression of 3D imaging data. The detectors of choice for camera-based 3D microscopy, including light-sheet microscopy, are currently 16-bit sCMOS cameras that generate data at a rate of about 800 MB s^{-1}. Having a large 16-bit dynamic range has practical benefits for avoiding detector saturation when imaging bright tissue regions while also ensuring that bit noise (that is, digitization noise) is not an issue when imaging dim tissue regions. However, the signal-to-noise ratio at any tissue region is generally much lower than 16 bits, owing to a combination of detector noise and shot noise (signal-induced and background-induced). This means that a substantial level of lossless compression can be achieved by windowing the dynamic range of the data to remove noise (at the low end) and unused pixel-well capacity (at the high end)[145]. For example, unlike lossy compression schemes (such as JPEG), which downsample the data in the Fourier or wavelet spaces, a recently developed B^3D compression scheme estimates the noise level of every pixel within an image (on the basis of neighbouring pixels) and limits the compression such that pixel deviations remain within that noise level[146]. With B^3D, fully lossless compression can be routinely achieved with an approximately 10× reduction in file size for the 16-bit imaging data generated by sCMOS camera-based light-sheet microscopy systems. In terms of speed, B^3D is built on the compute unified device architecture (CUDA) framework to enable graphics processing unit (GPU)-based compression of imaging data at high speeds (>1 GB s^{-1}), which surpasses the data rate of standard sCMOS cameras[146] (a similar algorithm, Jetraw, has been recently commercialized by Dotphoton). Depending on the image-analysis task at hand, the use of more advanced 3D compression methods that factor in the inherent redundancy of a 3D dataset could yield substantial data compression. In optical microscopy, most work on compression has been in two dimensions, even when applied to 3D datasets, as each slice is considered independently. However, other methods such as Fourier-based or wavelet-based compression could provide superior compression results for 3D datasets with acceptable trade-offs[147]. The effects of these various compression schemes on both manual and computational image-analysis routines needs to be examined further.

Visualization of image data. 3D pathology datasets are usually visualized as volume renderings or as a series of 2D cross-sectional views, depending on the diagnostic problem of interest and the complexity and density of the image. In some cases, it may be necessary to segment (that is, to extract) a subset of tissue structures using machine learning techniques in order to visualize the 3D structure in an informative way. For example, the ability to visualize a 3D mesh model of a vascular or glandular branching-tree network could yield key insights, including tortuosity, branching and other features that are not easily inferred from 2D images. Alternatively, it can also be helpful for pathologists to visualize 2D cross-sections of the same vessels or glands within the context of the surrounding cellular and stromal milieu, as is the case with standard H&E histology. In particular, because pathologists are currently trained to interpret 2D cross-sections, and a vast body of pathology literature exists for the characterization of diseases with 2D images, it is desirable to have both 2D and 3D visualizations. However, the time required to review large volumes of 3D data is often impractical. For example, in our experience, a prostate biopsy, which can be evaluated in two dimensions within a few minutes, can require 15–20 minutes for a thorough 3D evaluation[20]. Thus, in many cases, the full 3D dataset may only be necessary and practical to visualize in the case of diagnostic ambiguity, where it will have the largest clinical impact. In fact, early clinical implementations of 3D pathology may be as an adjunct to standard 2D pathology when diagnostic ambiguities arise or critical treatment decisions must be made; for example, for patients with prostate cancer with Gleason score 6–7, who must decide between active surveillance, surgery or radiation therapy. In summary, a variety of visualization techniques will need to be developed and standardized for pathologists to extract maximal utility from 3D pathology datasets. Figure 5 shows a number of examples of volume-rendered versus cross-sectional views of 3D pathology.

The ability to render 3D datasets with colour palettes that mimic conventional slide-based H&E histology and immunohistochemistry will be important to validate 3D pathology datasets and for pathologists to trust and adopt 3D pathology methods. Although fluorescence images from light-sheet microscopy and other forms of 3D microscopy are typically acquired using monochrome cameras (with the appropriate filters in place), it is possible to false-colour or pseudocolour the datasets to mimic the appearance of standard chromogenic stains when visualized by standard bright-field pathology microscopes. For example, it is possible to use the formulae for the Beer–Lambert law absorption of light to convert two-channel images of tissues (labelled with a fluorescent analogue of H&E) to H&E-like representations[19,20,56,77,78,148,149]. Similarly, 3D immunofluorescence images can be rendered to mimic conventional chromogenic immunohistochemistry[77]. The ability to create images that are familiar to pathologists is crucial for clinical adoption, so that pathologists can continue to rely on existing disease-classification schemes while learning how to improve their diagnostic determinations with the added insights that 3D pathology offers.

Open source tools for data processing, visualization and analysis. In the life cycle of all image datasets—research or clinical—software is used to acquire, visualize, analyse and disseminate results. For 3D microscopy data and for research purposes, there are currently a number of open source tools (in particular, the Fiji or ImageJ environment[150–152] and related applications such as MicroManager[153], BigDataViewer or BigStitcher[144,154], and Napari (https://github.com/napari/napari)) and closed source (commercial) software (such as Imaris, Amira, Arivis and Aivia). A growing movement within the imaging community advocates for the value of and need for open source workflows to ensure the reproducibility, transparency and broad dissemination of technology[155–158]. Since software tools undergo continuous development, and obtaining patent protection for software is difficult, many commercial entities have similarly opted for open source software suites, as they are typically well received by their customer base and can be used to support other technologies and devices that enjoy a stronger intellectual property position. The need for accuracy, transparency and reproducibility is particularly relevant in 3D pathology, owing to the large diversity of analysis parameters and metrics that are emerging and undergoing development. Access to well-curated cloud-hosted 3D pathology datasets, linked to common open source software, could accelerate the progress and standardization of image analysis tools in both academic and commercial sectors.

AI in 3D pathology. Rapid increases in computational power and the recent adoption of WSI scanners by multiple hospitals and healthcare institutions (which have started digitizing their entire pathology workflows) have led to the proliferation of digital pathology workflows in oncology and other clinical areas[18,159–161]. The term 'digital pathology' has become associated with AI, including machine learning techniques for the quantitative examination of whole-slide images to address clinical challenges in the early detection, diagnosis and prognosis of disease, and in the assessment and prediction of treatment responses. Although AI approaches have so far been developed mostly for the analysis of 2D pathology images, the advent of 3D pathology techniques has stimulated the development of 3D AI approaches for pathology. High-quality comprehensive 3D representations of tissue microarchitecture over large regions of interest offer a valuable opportunity for AI analyses owing to the large amounts of data that can be generated non-destructively from each patient specimen.

AI approaches in oncology aim primarily to develop a machine classifier for clinical decision support, such as identifying patients with early-stage disease who would benefit from aggressive therapeutic regimens such as adjuvant chemoradiotherapy[162], or identifying patients who are likely to respond to specific forms of therapy, such as immune-checkpoint blockade (for example, using PD-1 or PD-L1 inhibitors). Two commonly used classification approaches include end-to-end approaches and multistage techniques based on the extraction of hand-crafted features[163]. End-to-end strategies involve the training of a deep learning model to directly classify a lesion on the basis of imaging data. Such strategies are extremely powerful and accurate, but suffer in many cases from a lack of interpretability and the need for very large numbers of well-curated datasets to train a reliable algorithm. Improvements in data-efficient techniques, such as multiple-instance learning, semi-supervised learning and transfer learning, may help to mitigate the need for large training datasets[164–166]. However, variations in pre-analytic factors (such as those caused by staining quality, sectioning artefacts, out-of-focus regions and other subtle variations arising from the different scanners and scanning parameters used in pathology[18,167]) often make it difficult to create generalizable algorithms in the absence of sufficiently large training datasets that can capture the full diversity of the expected variations. In summary, deep learning models can be sensitive to minute (and often imperceptible) variations in image quality, where it is often difficult to spot errors when they occur and to determine the source of the errors[168]. Alternatively, image-processing methods (traditional or deep-learning-based) can be used to segment tissue structures (or primitives) that are already well known and trusted by pathologists (such as cells, nuclei, glands and collagen), from which intuitive features (such as density, tortuosity, fractal dimension and angular disorder) can be extracted. These quantitative histomorphometric features can then be used in a multistage approach to train a clinical classifier[169,170]. An advantage of such an approach is that domain experts (in this context, pathologists) can verify the accuracy of the intermediate segmentation steps, which facilitates the identification of errors and instils trust in the entire process. Another advantage of such a 'hand-crafted' approach is that each digital pathology

dataset typically contains large numbers of morphological primitives that can contribute to the training of an algorithm. Therefore, for low-level tasks (for instance, the segmentation of well-conserved microarchitectural structures), a modest number of patient specimens or training datasets is often sufficient[168,171–173]. A caveat with these approaches, however, is that they require a greater amount of domain-specific information for model training and might thus be more challenging to train than end-to-end approaches. Finally, an optimal classifier can be developed via hybrid approaches, such as using hand-crafted features as intermediate operators within a deep learning network, in conjunction with deep-learning-derived data-driven features[174,175].

Challenges for AI in 3D pathology. Deep-learning-based approaches for prognostic and predictive classification are increasingly being used in digital pathology (albeit largely for 2D pathology images). The challenge with 3D pathology images is that traditional 2D networks are not equipped to handle large 3D datasets. This will require 3D convolutional neural networks, which so far have been used mostly for the analysis and manipulation of (low-resolution) 3D radiographic images[176] at much smaller file sizes.

Beyond the computational expense of training 3D convolutional neural networks, additional challenges involve the definition of the training dataset and the annotation of regions or targets of interest. The need for manual annotation of structures and primitives in three dimensions by a domain expert will necessitate efficient and user-friendly interactive software. These tools will need to be flexible enough to allow the user to navigate through the 3D volume and to refine and update annotations of primitives and regions of interest. Although tools such as Sedeen (from Pathcore)[177] and QuPath[178] allow for object annotation of 2D pathology images, they require substantial modifications to accommodate the annotation of structures in large 3D pathology datasets. Alternatively, to bypass the requirements for laborious manual 3D annotations by domain experts, which is somewhat subjective, certain structures can be labelled using molecular biomarkers (for example, keratin 8 to identify the luminal epithelial cells that line all prostate glands and CD31 to highlight the lymphovasculature) such that traditional intensity-based and morphology-based segmentation methods can be more reliably employed. Although this molecular labelling approach is objective and may bypass the need for manual annotations, one downside is that the antibody-based labelling of thick 3D tissues can be very slow and expensive. However, if a deep learning model can be trained to predict the appearance of 3D immunofluorescence staining on the basis of images generated with inexpensive and fast small-molecule fluorophores (for example, an H&E analogue), or even without the use of labels[171,172,179,180], it should be possible to develop an annotation-free segmentation algorithm based on synthetic immunolabelling of specific structures. Such a method would be objective (no human annotations needed), fast (as it could rely on small-molecule labels that diffuse rapidly in thick tissues) and inexpensive (because it would be antibody-free).

Quality control in AI-based analysis. An important factor influencing the performance of AI in digital pathology is the inherent quality of the data fed into the algorithms. AI analysis of 2D pathology is often limited by pre-analytic sources of variation. Although the sources of image variability are different for non-destructive 3D pathology, there is a similar need to control for such variations when it comes to implementing AI approaches. For example, factors that can influence the quality of 3D pathology include the degree of fixation, cold and warm ischaemia times, deparaffinization quality (if FFPE blocks are being used), variations in staining and in clearing protocols, fluctuations in laser intensities, optical alignment and software post-processing routines. In 3D microscopy, images are typically always in focus, provided that the alignment of the microscope is maintained. Image quality is therefore most influenced by tissue preparation. As with slide-based histology, the automation of tissue-preparation steps can reduce variability, but quality control metrics are still needed to ensure that 3D pathology datasets are reliable for AI-based analyses. Automated and semi-automated quality control methods for 2D WSI, which can be modified for 3D pathology, aim to automatically detect variations in colour and in staining as well as common artefacts present in histology images. One such tool is HistoQC[181], which interrogates digital tissue-slide images and provides a quantitative score of the overall image quality. The software also enables the precise identification of localized regions that have been compromised by artefacts, such as cracks in the glass, hair shafts, tissue folds and pen markings. Similar tools will need to be extended for the quality control of 3D pathology images, for which image artefacts include stitching defects and regions of poor staining or clearing.

Some level of variation in image quality is unavoidable in 2D and 3D pathology, regardless of the degree of automation and process standardization. Nevertheless, a hand-crafted feature-based AI approach for image interpretation would offer advantages. First, it could find histomorphometric features that are relatively insensitive to variations in image quality, as exemplified by a recent sensitivity analysis that identified a subset of quantitative features in 2D pathology images that could be integrated into robust clinical classifiers[182]. Second, segmentation algorithms (for the extraction of quantitative features) can be trained with diverse datasets such that

Fig. 5 | Non-destructive 3D pathology of clinical specimens. a, Twelve core-needle biopsies from the prostate of a single patient, imaged comprehensively in three dimensions with an OTLS microscopy system[77]. The specimen was labelled with a fluorescent analogue of H&E staining, and pseudocoloured to mimic the appearance of standard H&E histology. **b**, Benign and malignant glands were easily identified, with significant variations in appearance as a function of depth, which suggests that 3D pathology may improve the diagnosis and grading of prostate carcinoma[19,20]. **c**, A bladder cancer FFPE specimen was deparaffinized, cleared (right), fluorescently labelled for nuclei and N-cadherin, and then imaged by light-sheet microscopy[43] (left). Scale bars, 80 μm (yellow) and 1,600 μm (cyan, red). Pseudo, pseudocoloured. **d**, A number of vascular features (tortuosity, radius and density kurtosis) for 45 human bladder specimens, showing significant differences (asterisks) across normal specimens (blue), specimens with a non-muscle-invasive tumour where the pathological stage is less than T2 (< pT2, green) and specimens with a muscle-invasive tumour (≥ pT2, red)[43]. These quantitative vascular features were obtained after segmenting out the vessel network. **e**, Renderings of light-sheet microscopy data of a CD34-immunolabelled tumour[43]. Individual blood vessels (thin, blue; thick, red) of the 3D vascular network can be appreciated at both low magnification (bottom left) and at high magnification (right). Scale bars, 80 μm. **f**, A receiver-operating-characteristic (ROC) analysis for the ability to detect muscle-invasive versus muscle-non-invasive tumour showed that 3D vascular features outperform 2D features, and that combining all 3D features yielded the best performance[43]. **g**, Multiplexed 3D immunofluorescence imaging with confocal microscopy of intact core-needle biopsies of cancer[45]. **h**, Normalized densities of $CD3^+CD8^+$ cytotoxic lymphocytes (CTLs) and of $CD31^+$ microvasculature in $EGFR^+$ (epidermal growth-factor receptor) parenchyma were used to cluster human tumours into inflamed and non-inflamed phenotypes. P, patient. **i**, The 3D spatial mapping of an inflamed patient sample revealed that over 54% of $CD3^+CD8^+$ CTLs were located within 10 μm of microvessels[45]. The inset shows a colour map that denotes distance from a blood vessel, where the arrow indicates the distance from the vessel surface and the surface of a CTL. Figure reproduced from: **a**, ref. [77], under a CC BY 4.0 licence; **c**,**f**, ref. [43], Springer Nature Ltd; **h**,**i**, ref. [45], Springer Nature Ltd. Figure adapted from: **d**,**e**, ref. [43], Springer Nature Ltd; **g**, ref. [45], Springer Nature Ltd.

they are robust against image quality variations. Although this is also possible with an end-to-end classification approach if sufficient numbers of patient datasets are available for algorithm training, the use of a hand-crafted approach would allow pathologists to visually inspect the results at a critical intermediate step (the segmentation of tissue structures). In addition, since each 3D pathology dataset

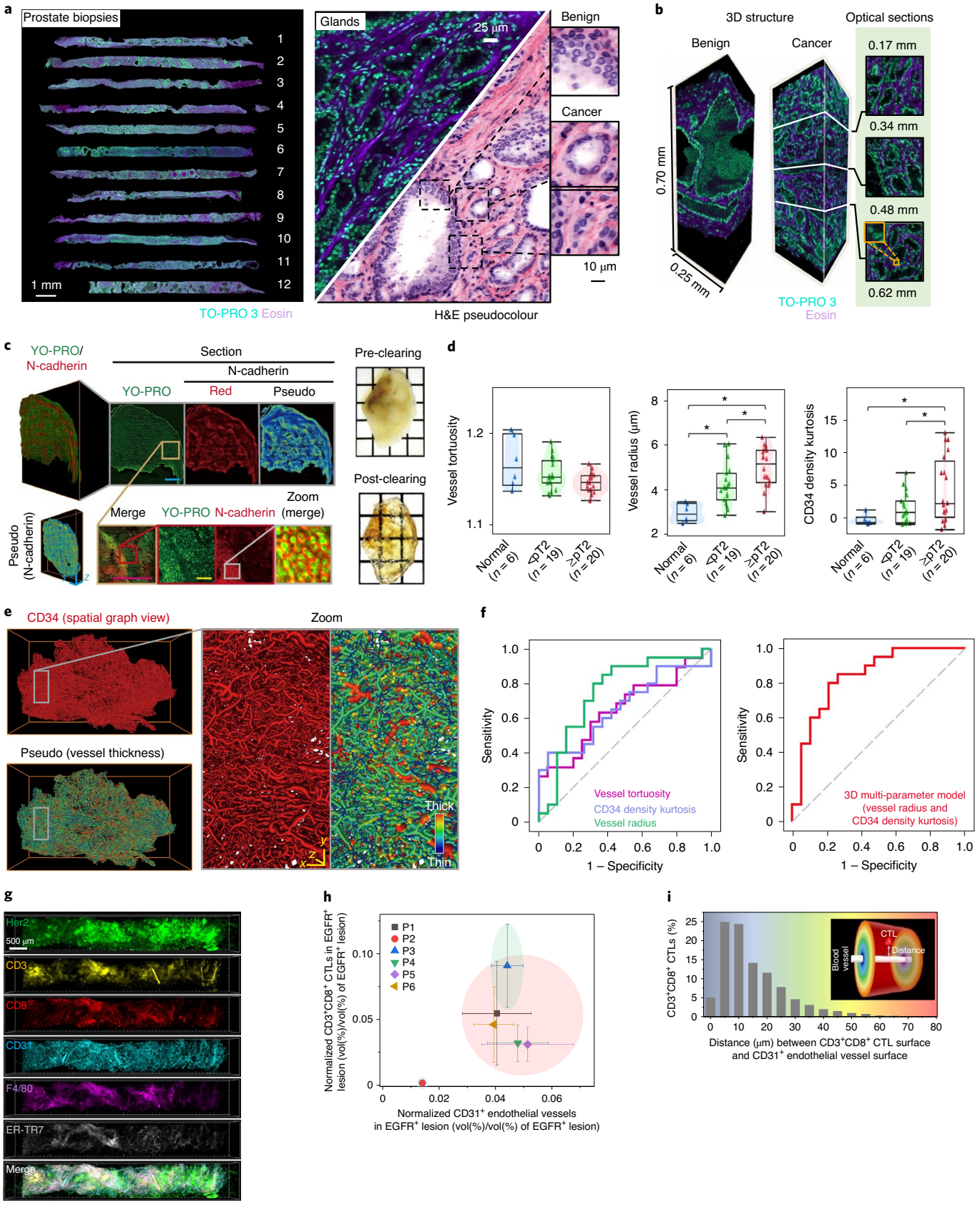

often contains hundreds to thousands of diverse examples of various primitives (basic structures), smaller patient cohorts could be used to accurately train the algorithms to segment such structures (such as glands, collagen, nuclei and broad classes of cells).

Challenges for clinical adoption

There are substantial technical, regulatory and financial challenges to overcome for the clinical adoption of 3D pathology.

Clinical studies with archived tissues. In contrast to clinical trials involving therapeutics, for which new patients must be recruited and followed over time, new technologies in pathology can often be validated using established slide repositories or tissue biobanks with detailed follow-up data (such as The Cancer Genome Atlas[183] and the Prostate Cancer Biorepository Network (http://prostatebiorepository.org)). These biobanks permit prospective–retrospective study designs. For instance, a 21-gene expression assay using FFPE tissue, the Oncotype DX Recurrence Score by Genomic Health, was validated using archived specimens from the National Surgical Adjuvant Breast and Bowel Project (NSABP) trials B14 and B20[184,185]. These randomized clinical trials were completed more than a decade before the validation of Oncotype DX, enabling the use of 10 year recurrence-free survival as the primary endpoint, and thus reinforcing the value of well-characterized archival tissue in translating promising diagnostic technologies to the clinic[186]. However, pre-analytic factors (such as formalin fixation time, cold ischaemia time and freezing methodology) all affect the quality of tissue stored in a biobank[187]. If the effects of these pre-analytic factors are severe, the assay can be negatively impacted, or samples must be removed from the study, which can introduce bias. An additional concern with the use of archival tissue is that standard-of-care treatments for the target population could have changed over time, which could potentially confound studies in which the primary endpoints are clinical outcomes rather than biological measurements. To further extend the example of the Oncotype DX Recurrence Score, the assay was later validated by a prospective randomized trial (TAILORx), which reinforced the value of the test[188]. The cumulative body of evidence, including prospective–retrospective studies and prospective randomized studies, led to the categorization of the Oncotype DX Recurrence Score as the only preferred test in the 2018 National Comprehensive Cancer Network (NCCN) treatment guidelines for a specific subset of patients with breast cancer (early-stage hormone-positive node-negative) facing a chemotherapy decision, which is the highest level of clinical acceptance.

Regulatory strategies. The development of 3D pathology implementations that can meet the requirements for regulatory approval will require close collaboration with relevant regulatory stakeholders, such as the United States Food and Drug Administration (FDA). Below, we provide a high-level overview of potential regulatory scenarios, along with examples from devices and diagnostic approaches that are currently in the market. There are two primary regulatory pathways in the United States for diagnostic tests in pathology: FDA approval and laboratory-developed tests[189] (LDTs).

Diagnostic tests and kits are classified as medical devices by the FDA, and are subject to the same regulatory processes as other such devices. Medical devices are categorized according to the perceived level of risk for their intended use, from class I to class III. Class III devices carry the highest risk, and include implanted devices and those that are used to sustain life. Class II devices are considered to have moderate-to-high risk, and have a predicate device that can be used for comparison. For example, a whole-slide scanner for 2D digital pathology was first approved by the FDA in 2017 as a class II device, after an extensive clinical study, for an intended use of primary diagnosis[190,191]. Class I devices are the lowest-risk devices, which include the analogue light microscopes used in pathology laboratories. A recent microscopy device for use with ex vivo tissue (the Caliber ID Vivascope 2500) was classified as a class I device.

For many diagnostic assays, the LDT regulatory pathway can be an alternative if the test is provided as a medical service by a single laboratory. Tests designated as LDTs must be performed in a Clinical Laboratory Improvement Amendments (CLIA)-certified laboratory with appropriate analytic and clinical validation documentation. The FDA does not currently regulate LDTs, but in recent years has expressed its intentions to issue an oversight framework for them[192,193].

The regulatory strategy for 3D pathology will be largely dependent on how the technology is disseminated. If the technology is developed as a device that is marketed to pathology laboratories, FDA approval will be necessary for use of the device, and potentially for decision-support algorithms based on the device. If individual laboratories develop customized 3D pathology tests, the LDT pathway could be a viable option. Regardless of the regulatory pathway and the world region in which it is implemented (regulatory pathways may differ markedly by country), a strong base of evidence for clinical utility will be crucial for the adoption of 3D pathology.

Financial considerations. The workflows for conventional pathology and 3D pathology are similar, at least for the accessioning, grossing and initial tissue-processing steps (that is, fixation and dehydration). The differences begin after the tissue is embedded in paraffin (conventional pathology) or placed in the clearing solution. In a conventional pathology workflow, the tissue must be physically sectioned (by hand), placed on a glass slide, stained, cover-slipped and scanned using a whole-slide imager to produce a digital 2D dataset. Using a set of 12 prostate biopsies as an example, this process requires about 40 minutes of hands-on histotechnologist time, about 4 hours of total time and about US$300,000 in capital equipment costs. In the 3D pathology workflow, automated tissue scanning using light-sheet microscopy with similar resolution to that provided by a 10× to 20× objective (NA around 0.4) in a standard pathology microscope requires roughly 30 minutes (if 10% of the sample is digitized) to about 4 hours (if 100% of the sample is digitized)[77]. Because manual sectioning is not required, the 3D pathology workflow can be entirely automated, and thus does not depend on timing of labour shifts or on the availability of histotechnologists. The capital equipment costs are likely to be similar for 2D and 3D pathology (currently, there are no FDA-approved devices for 3D pathology). Hence, the 3D pathology workflow can reduce the labour burden on histotechnologists while non-destructively generating orders of magnitude more data than a whole-slide imager.

AI-enabled pathology workflows. Although a fully automated diagnostic and decision-support workflow for pathology could become a reality, the integration of AI will probably occur in a stepwise fashion (Fig. 6). For 3D pathology, this integration will probably entail at least three stages, starting with the direct interpretation of 3D image datasets by pathologists. This first step is time-intensive but is the least risky, because datasets could be rendered to mimic the current standards of H&E histology and immunohistochemistry and would be viewed much like 2D whole-slide images, albeit with the ability to scroll through the depth of a specimen. There is preliminary evidence that such a strategy could be highly informative, in particular for preventing the over-grading (and consequent overtreatment) of disease[19] and for identifying regions of malignancy that could be missed or misinterpreted with slide-based 2D histology[20]. Similarly, the sampling limitations and ambiguity of 2D histology are known to lead to misdiagnosis and under-grading of certain patients[194–196], which presents an opportunity for 3D pathology to improve on the standard of care. Because 3D assessments of tissue (entire biopsies, in particular) are more time consuming than 2D assessments of sparse 2D sections, a second stage of integration

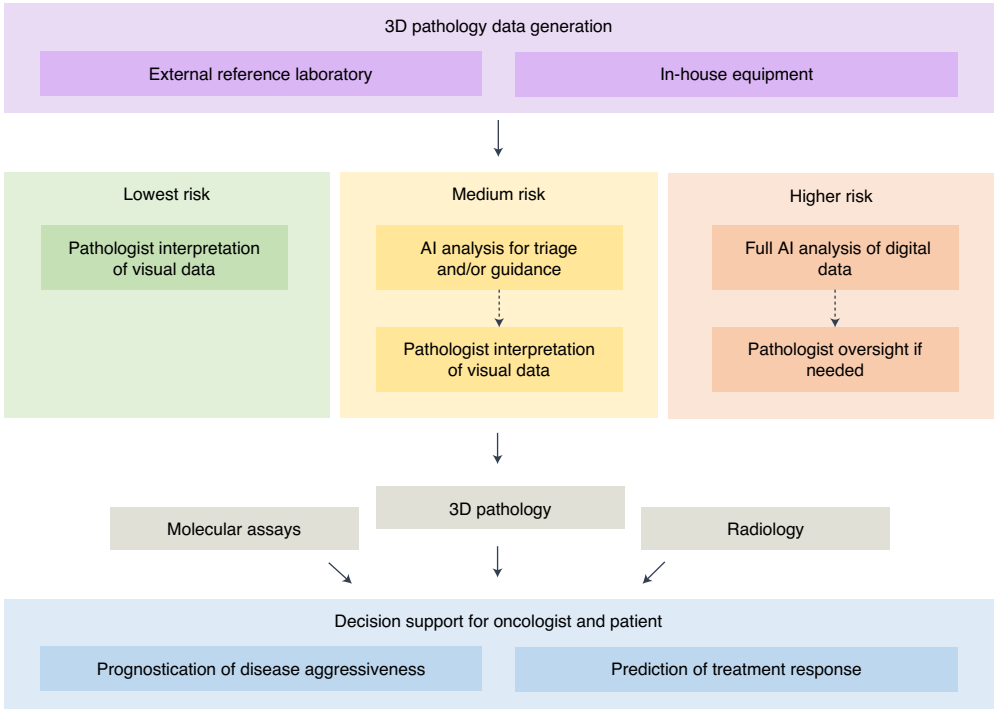

Fig. 6 | Implementing 3D pathology in clinical practice. 3D pathology datasets, generated by reference laboratories or by in-house pathology laboratories, may initially provide additional visual information for pathologists as they seek to improve their diagnostic determinations. The early low-risk incorporation of AI analysis will probably involve the triaging of unambiguous cases to reduce the workload of pathologists and guide their efforts towards regions of ambiguity and diagnostic importance. As AI algorithms are increasingly validated and trusted by clinicians, they may eventually be used for the fully automated analysis of 3D pathology datasets, with optional oversight by a pathologist. The overarching vision for 3D pathology is to provide clinical decision support (prognostication and prediction) to guide treatment decisions, ideally in conjunction with other molecular and imaging assays.

could use AI to automatically triage diagnostically unambiguous specimens, with only ambiguous cases requiring interpretation by a pathologist. For example, with 2D digital pathology images it may be possible to triage up to 75% of cancer cases on the basis of computational analysis while retaining 100% detection sensitivity[197]. As clinical studies prove their effectiveness, fully automated computational 3D pathology workflows may emerge. Moreover, 3D pathology will need to seamlessly be integrated into laboratory information management systems such that various sources of patient data can be used by clinicians and by AI algorithms.

Future directions

There are substantial opportunities in the integration of 3D pathology with molecular assays, in the co-registration of multiscale imaging data, and in the use of 3D pathology to reduce healthcare disparities and aid decision-support systems.

Integration with molecular assays. Precision medicine will undoubtedly benefit from adopting an approach that combines multiplexed and multiomics diagnostic technologies for patient stratification and clinical decision support. In particular, the complexities of the tumour immune microenvironment, and the various factors that contribute to an individual's inherent immunological status (recently referred to as the cancer-immune set point) are critical factors to take into account when driving improvements in immuno-oncology[198]. For example, factors that correlate with the response to immune-checkpoint blockade include the tumour's mutational burden[199], microbiome profiles[200,201], patterns of expression of biomarkers (such as PD-1, PD-L1 and chemokine receptors)[12,202,203], and the spatial distribution of tumour cells and immune cells (that is, tumour-infiltrating lymphocytes)[204]. To facilitate the integration of 3D pathology with other clinical assays such as DNA or RNA sequencing, a first step is to ensure that 3D pathology methods do not interfere with standard laboratory methods. Certain clearing and fluorescence-labelling methods are relatively gentle, and often use reagents (such as xylene and ethanol) that are already part of the standard histology workflow. Once tissues have been formalin-fixed per standard clinical practice, most clearing reagents are less harsh than the initial fixation step, and standard FFPE processing and histology assays can still be performed. Modernization of pathology workflows will follow, for example by developing formalin-free tissue-preservation methods as well as labelling and clearing protocols that can maintain RNA integrity. 3D analogues to existing pathology practices, such as laser-capture microdissection and the manual slide-based macrodissection of tissues, would also be of value. Such 3D tissue-enrichment techniques could generate orders of magnitude more material for downstream assays than slide-based tissue shavings and laser-captured regions, which could result in a significant leap in sensitivity and accuracy for detecting rare mutations. For rare cell types, the 3D microaspiration of individual cells or cell contents within thick specimens is also a possibility, as shown in a neuroscience context[205–207]. The ability to extract lysates from tens to hundreds of individual rare cells—such as aggressive tumour cells exhibiting lymphovascular invasion—followed by the low-input sequencing of those lysates, could enable the discovery of new biomarkers of aggressive disease (for prognostication), druggable targets or mechanistic insights.

Co-registration of multiscale imaging data. Modern 3D pathology, when deployed with the types of computational tools that radiography has pioneered, could provide a cell-to-organ view that is not possible with any other currently available clinical imaging strategy. The co-registration of conventional 2D pathology with medical images for the improved characterization of diseases over a

large range of spatial scales[208–211] is motivated most often by the use of pathology as a gold standard to confirm changes seen at macroscopic tissue scales with whole-body imaging methods[212]. For example, in current clinical practice, radiology techniques are often used for the early detection of various diseases, where histopathology is subsequently relied on to provide diagnostic, prognostic and predictive insights. Pathology and radiology approaches are also often used for cross-validation. For example, PET imaging results have been correlated with histologically determined metrics such as proliferative index (Ki-67 expression), microvessel density and immune phenotype[213–215] (in particular, CD8 expression). However, correlative studies would benefit from increased standardization in medical imaging and histopathology. Previous efforts to standardize the co-registration of radiology and pathology approaches include placing fiducial markers to guide ex vivo mould-based tissue slicing[216]. 3D reconstructions of 2D pathology data have also been generated to improve registration accuracy[209]. The emergence of non-destructive 3D pathology, which can enable the visualization of large tissue volumes, has the potential to greatly facilitate and improve co-registration with radiographic images. In addition, preclinical imaging modalities such as micro-CT, MRI or PET may be helpful to bridge large gaps in spatial resolution and volumetric field between microscopy and whole-body imaging techniques[217].

Mitigation of healthcare disparities. Histomorphometric features of cancer can exhibit population-level differences. For instance, a recent study of H&E-stained whole-slide images showed that stromal features of prostate cancer differed significantly between African American and white American men, and a computational prognostic model trained with these stromal features strongly predicted risk of recurrence in two independent validation datasets of African American men[169]. Interestingly, this prognostic model, which was trained with data from African American men alone, was nearly twice as accurate than a model trained with a combination of data from both African American and white American men. Considering that significant 2D morphometric differences have been identified between African American and white American men with prostate cancer, there is optimism that the computational interrogation of 3D stromal and epithelial morphology can further improve the treatment of disparate populations. This includes those who have traditionally been underserved, such as African American men with prostate cancer, whose mortality rate in the United States is nearly 2.5 times that of white men with prostate cancer[218].

Holistic decision-support algorithms. Recent research has expanded from interrogating a single source of information (such as radiology, pathology, genomics or metabolomics) to merging data from multiple modalities in a bid to improve prognostication and prediction. This is an especially attractive approach for AI-based methods that thriveon large amounts of orthogonal and complementary data. AI-based integration of multiple data types has already been used in cancers of the lung[219,220], breast[221,222], brain[223] and prostate[224], as well as for cardiovascular[225] and neurological diseases[226]. These examples indicate that holistically combining data from various diagnostic modalities and patient records can yield accurate decision-support algorithms (Fig. 6).

Outlook

Many technologies in radiology have been developed and refined over the past five decades, yet pathology remains rooted in over a century of tradition. However, the fact that pathology is still regarded as the gold standard for clinical diagnosis attests to the wealth of insight that tissue microscopy offers, even when obtained from small numbers of thin 2D sections. The recent FDA approval of digital pathology solutions indicates that pathology is entering a phase of modernization that will continue to evolve over the next half century. This advent of 2D WSI will pave the way for non-destructive 3D pathology; for example, by establishing the clinical information technology infrastructure and resources needed to support a digital 3D pathology workflow. In many ways, non-destructive 3D pathology represents the ultimate and ideal fulfilment of the vision for digital pathology. Just as digital X-ray and X-ray CT imaging at the end of the twentieth century enabled analogue film to be replaced by reusable X-ray panels, with strong economic benefits[227], non-destructive 3D pathology similarly offers the potential to bypass the use of glass slides and associated tissue-sectioning processes in favour of a simpler digital approach that generates superior data. Convenience and cost savings alone may not provide sufficient motivation to drive the rapid adoption of 3D pathology, but clear advantages that improve clinical outcomes may tilt the balance.

Received: 9 January 2020; Accepted: 17 December 2020;
Published online: 15 February 2021

References

1. Carroll, P. R. et al. NCCN guidelines insights: prostate cancer early detection, version 2.2016. *J. Natl Compr. Canc. Netw.* **14**, 509–519 (2016).
2. Gradishar, W. J. et al. NCCN guidelines insights: breast cancer, version 1.2016. *J. Natl Compr. Canc. Netw.* **13**, 1475–1485 (2015).
3. McKenney, J. K. et al. The potential impact of reproducibility of Gleason grading in men with early stage prostate cancer managed by active surveillance: a multi-institutional study. *J. Urol.* **186**, 465–469 (2011).
4. Shah, R. B. et al. Diagnosis of Gleason pattern 5 prostate adenocarcinoma on core needle biopsy: an interobserver reproducibility study among urologic pathologists. *Am. J. Surg. Pathol.* **39**, 1242–1249 (2015).
5. Zhou, M. et al. Diagnosis of 'poorly formed glands' Gleason pattern 4 prostatic adenocarcinoma on needle biopsy: an interobserver reproducibility study among urologic pathologists with recommendations. *Am. J. Surg. Pathol.* **39**, 1331–1339 (2015).
6. Kweldam, C. F. et al. Gleason grade 4 prostate adenocarcinoma patterns: an interobserver agreement study among genitourinary pathologists. *Histopathology* **69**, 441–449 (2016).
7. Epstein, J. I. et al. A contemporary prostate cancer grading system: a validated alternative to the Gleason score. *Eur. Urol.* **69**, 428–435 (2016).
8. Welch, H. G. & Black, W. C. Overdiagnosis in cancer. *J. Natl Cancer Inst.* **102**, 605–613 (2010).
9. Haffner, M. C., De Marzo, A. M., Yegnasubramanian, S., Epstein, J. I. & Carter, H. B. Diagnostic challenges of clonal heterogeneity in prostate cancer. *J. Clin. Oncol.* **33**, e38–e40 (2015).
10. Meyers, D. E., Bryan, P. M., Banerji, S. & Morris, D. G. Targeting the PD-1/PD-L1 axis for the treatment of non-small-cell lung cancer. *Curr. Oncol.* **25**, e324–e334 (2018).
11. Hersom, M. & Jørgensen, J. T. Companion and complementary diagnostics-focus on PD-L1 expression assays for PD-1/PD-L1 checkpoint inhibitors in non-small cell lung cancer. *Ther. Drug Monit.* **40**, 9–16 (2018).
12. Patel, S. P. & Kurzrock, R. PD-L1 expression as a predictive biomarker in cancer immunotherapy. *Mol. Cancer Ther.* **14**, 847–856 (2015).
13. Brunnström, H. et al. PD-L1 immunohistochemistry in clinical diagnostics of lung cancer: inter-pathologist variability is higher than assay variability. *Mod. Pathol.* **30**, 1411–1421 (2017).
14. Makhlouf, H. et al. Toward improving practices for submission of diagnostic tissue blocks for National Cancer Institute clinical trials. *Am. J. Clin. Pathol.* **153**, 149–155 (2020).
15. Olson, E., Levene, M. J. & Torres, R. Multiphoton microscopy with clearing for three dimensional histology of kidney biopsies. *Biomed. Opt. Express* **7**, 3089–3096 (2016).
16. Paul, D., Cowan, A. E., Ge, S. & Pachter, J. S. Novel 3D analysis of claudin-5 reveals significant endothelial heterogeneity among CNS microvessels. *Microvasc. Res.* **86**, 1–10 (2013).
17. Torres, R. et al. Three-dimensional morphology by multiphoton microscopy with clearing in a model of cisplatin-induced CKD. *J. Am. Soc. Nephrol.* **27**, 1102–1112 (2016).
18. Bera, K., Schalper, K. A., Rimm, D. L., Velcheti, V. & Madabhushi, A. Artificial intelligence in digital pathology—new tools for diagnosis and precision oncology. *Nat. Rev. Clin. Oncol.* **16**, 703–715 (2019).
19. Glaser, A. K. et al. Light-sheet microscopy for slide-free non-destructive pathology of large clinical specimens. *Nat. Biomed. Eng.* **1**, 0084 (2017).
20. Reder, N. P. et al. Open-top light-sheet microscopy image atlas of prostate core needle biopsies. *Arch. Pathol. Lab. Med.* **143**, 1069–1075 (2019).

21. Johnson, D. B. et al. Quantitative spatial profiling of PD-1/PD-L1 interaction and HLA-DR/IDO-1 predicts improved outcomes of anti-PD-1 therapies in metastatic melanoma. *Clin. Cancer Res.* **24**, 5250–5260 (2018).
22. Kargl, J. et al. Neutrophils dominate the immune cell composition in non-small cell lung cancer. *Nat. Commun.* **8**, 14381 (2017).
23. He, G. et al. Peritumoural neutrophils negatively regulate adaptive immunity via the PD-L1/PD-1 signalling pathway in hepatocellular carcinoma. *J. Exp. Clin. Cancer Res.* **34**, 141 (2015).
24. Yuan, Y. Spatial heterogeneity in the tumor microenvironment. *Cold Spring Harb. Perspect. Med.* **6**, a026583 (2016).
25. Masugi, Y. et al. Characterization of spatial distribution of tumor-infiltrating $CD8^+$ T cells refines their prognostic utility for pancreatic cancer survival. *Mod. Pathol.* **32**, 1495–1507 (2019).
26. Heindl, A., Nawaz, S. & Yuan, Y. Mapping spatial heterogeneity in the tumor microenvironment: a new era for digital pathology. *Lab. Investig.* **95**, 377–384 (2015).
27. Plaks, V., Kong, N. & Werb, Z. The cancer stem cell niche: how essential is the niche in regulating stemness of tumor cells? *Cell Stem Cell* **16**, 225–238 (2015).
28. Guo, W. et al. Multi-genetic events collaboratively contribute to *Pten*-null leukaemia stem-cell formation. *Nature* **453**, 529–533 (2008).
29. Adams, J. M. & Strasser, A. Is tumor growth sustained by rare cancer stem cells or dominant clones? *Cancer Res.* **68**, 4018–4021 (2008).
30. Cavé, H. et al. Clinical significance of minimal residual disease in childhood acute lymphoblastic leukemia. *N. Engl. J. Med.* **339**, 591–598 (1998).
31. van Dongen, J. J. et al. Prognostic value of minimal residual disease in acute lymphoblastic leukaemia in childhood. *Lancet* **352**, 1731–1738 (1998).
32. Herman, C. M., Wilcox, G. E., Kattan, M. W., Scardino, P. T. & Wheeler, T. M. Lymphovascular invasion as a predictor of disease progression in prostate cancer. *Am. J. Surg. Pathol.* **24**, 859–863 (2000).
33. Mohammed, R. A. A. et al. Improved methods of detection of lymphovascular invasion demonstrate that it is the predominant method of vascular invasion in breast cancer and has important clinical consequences. *Am. J. Surg. Pathol.* **31**, 1825–1833 (2007).
34. Song, Y. J. et al. The role of lymphovascular invasion as a prognostic factor in patients with lymph node-positive operable invasive breast cancer. *J. Breast Cancer* **14**, 198–203 (2011).
35. Haffner, M. C. et al. Tracking the clonal origin of lethal prostate cancer. *J. Clin. Investig.* **123**, 4918–4922 (2013).
36. Pribluda, A., de la Cruz, C. C. & Jackson, E. L. Intratumoral heterogeneity: from diversity comes resistance. *Clin. Cancer Res.* **21**, 2916–2923 (2015).
37. Eyler, C. E. & Rich, J. N. Survival of the fittest: cancer stem cells in therapeutic resistance and angiogenesis. *J. Clin. Oncol.* **26**, 2839–2845 (2008).
38. Brooks, M. D., Burness, M. L. & Wicha, M. S. Therapeutic implications of cellular heterogeneity and plasticity in breast cancer. *Cell Stem Cell* **17**, 260–271 (2015).
39. Humphrey, P. A. Complete histologic serial sectioning of a prostate gland with adenocarcinoma. *Am. J. Surg. Pathol.* **17**, 468–472 (1993).
40. McCormick, B. H. et al. Construction of anatomically correct models of mouse brain networks. *Neurocomputing* **58–60**, 379–386 (2004).
41. Li, A. et al. Micro-optical sectioning tomography to obtain a high-resolution atlas of the mouse brain. *Science* **330**, 1404–1408 (2010).
42. van Royen, M. E. et al. Three-dimensional microscopic analysis of clinical prostate specimens. *Histopathology* **69**, 985–992 (2016).
43. Tanaka, N. et al. Whole-tissue biopsy phenotyping of three-dimensional tumours reveals patterns of cancer heterogeneity. *Nat. Biomed. Eng.* **1**, 796–806 (2017).
44. Tanaka, N. et al. Mapping of the three-dimensional lymphatic microvasculature in bladder tumours using light-sheet microscopy. *Br. J. Cancer* **118**, 995–999 (2018).
45. Lee, S. S.-Y., Bindokas, V. P., Lingen, M. W. & Kron, S. J. Nondestructive, multiplex three-dimensional mapping of immune infiltrates in core needle biopsy. *Lab. Invest.* **99**, 1400–1413 (2019).
46. Verhoef, E. I. et al. Three-dimensional analysis reveals two major architectural subgroups of prostate cancer growth patterns. *Mod. Pathol.* **32**, 1032–1041 (2019).
47. Pierce, M. C., Javier, D. J. & Richards-Kortum, R. Optical contrast agents and imaging systems for detection and diagnosis of cancer. *Int. J. Cancer* **123**, 1979–1990 (2008).
48. Abeytunge, S., Li, Y., Larson, B., Toledo-Crow, R. & Rajadhyaksha, M. Rapid confocal imaging of large areas of excised tissue with strip mosaicing. *J. Biomed. Opt.* **16**, 050504 (2011).
49. Abeytunge, S. et al. Confocal microscopy with strip mosaicing for rapid imaging over large areas of excised tissue. *J. Biomed. Opt.* **18**, 61227 (2013).
50. Tao, Y. K. et al. Assessment of breast pathologies using nonlinear microscopy. *Proc. Natl Acad. Sci. USA* **111**, 15304–15309 (2014).
51. Ji, M. et al. Detection of human brain tumor infiltration with quantitative stimulated Raman scattering microscopy. *Sci. Transl. Med* **7**, 309ra163 (2015).
52. Orringer, D. A. et al. Rapid intraoperative histology of unprocessed surgical specimens via fibre-laser-based stimulated Raman scattering microscopy. *Nat. Biomed. Eng.* **1**, 0027 (2017).
53. Abeytunge, S. et al. Evaluation of breast tissue with confocal strip-mosaicking microscopy: a test approach emulating pathology-like examination. *J. Biomed. Opt.* **22**, 34002 (2017).
54. Boppart, S. A. et al. Label-free optical imaging technologies for rapid translation and use during intraoperative surgical and tumor margin assessment. *J. Biomed. Opt.* **23**, 021104 (2017).
55. Yoshitake, T. et al. Rapid histopathological imaging of skin and breast cancer surgical specimens using immersion microscopy with ultraviolet surface excitation. *Sci. Rep.* **8**, 4476 (2018).
56. Chen, Y. et al. Rapid pathology of lumpectomy margins with open-top light-sheet (OTLS) microscopy. *Biomed. Opt. Express* **10**, 1257–1272 (2019).
57. Liu, J. T. C. et al. Micromirror-scanned dual-axis confocal microscope utilizing a gradient-index relay lens for image guidance during brain surgery. *J. Biomed. Opt.* **15**, 026029 (2010).
58. Sanai, N. et al. Intraoperative confocal microscopy in the visualization of 5-aminolevulinic acid fluorescence in low-grade gliomas. *J. Neurosurg.* **115**, 740–748 (2011).
59. Nguyen, Q. T. & Tsien, R. Y. Fluorescence-guided surgery with live molecular navigation—a new cutting edge. *Nat. Rev. Cancer* **13**, 653–662 (2013).
60. Wei, L., Roberts, D. W., Sanai, N. & Liu, J. T. C. Visualization technologies for 5-ALA-based fluorescence-guided surgeries. *J. Neurooncol.* **141**, 495–505 (2019).
61. Wei, L., Fujita, Y., Sanai, N. & Liu, J. T. C. Toward quantitative neurosurgical guidance with high-resolution microscopy of 5-aminolevulinic acid-induced protoporphyrin IX. *Front. Oncol.* **9**, 592 (2019).
62. Thawani, R. et al. Radiomics and radiogenomics in lung cancer: a review for the clinician. *Lung Cancer* **115**, 34–41 (2018).
63. Lambin, P. et al. Radiomics: the bridge between medical imaging and personalized medicine. *Nat. Rev. Clin. Oncol.* **14**, 749–762 (2017).
64. Richardson, D. S. & Lichtman, J. W. Clarifying tissue clearing. *Cell* **162**, 246–257 (2015).
65. Azaripour, A. et al. A survey of clearing techniques for 3D imaging of tissues with special reference to connective tissue. *Prog. Histochem. Cytochem.* **51**, 9–23 (2016).
66. Berke, I. M., Miola, J. P., David, M. A., Smith, M. K. & Price, C. Seeing through musculoskeletal tissues: improving in situ imaging of bone and the lacunar canalicular system through optical clearing. *PLoS ONE* **11**, e0150268 (2016).
67. Jing, D. et al. Tissue clearing of both hard and soft tissue organs with the PEGASOS method. *Cell Res.* **28**, 803–818 (2018).
68. Hama, H. et al. ScaleS: an optical clearing palette for biological imaging. *Nat. Neurosci.* **18**, 1518–1529 (2015).
69. Ke, M.-T., Fujimoto, S. & Imai, T. SeeDB: a simple and morphology-preserving optical clearing agent for neuronal circuit reconstruction. *Nat. Neurosci.* **16**, 1154–1161 (2013).
70. Chung, K. et al. Structural and molecular interrogation of intact biological systems. *Nature* **497**, 332–337 (2013).
71. Susaki, E. A. et al. Whole-brain imaging with single-cell resolution using chemical cocktails and computational analysis. *Cell* **157**, 726–739 (2014).
72. Kim, S.-Y. et al. Stochastic electrotransport selectively enhances the transport of highly electromobile molecules. *Proc. Natl Acad. Sci. USA* **112**, E6274–E6283 (2015).
73. Miyawaki, T. et al. Visualization and molecular characterization of whole-brain vascular networks with capillary resolution. *Nat. Commun.* **11**, 1104 (2020).
74. Renier, N. et al. iDISCO: a simple, rapid method to immunolabel large tissue samples for volume imaging. *Cell* **159**, 896–910 (2014).
75. Klingberg, A. et al. Fully automated evaluation of total glomerular number and capillary tuft size in nephritic kidneys using lightsheet microscopy. *J. Am. Soc. Nephrol.* **28**, 452–459 (2017).
76. Silvestri, L., Costantini, I., Sacconi, L. & Pavone, F. S. Clearing of fixed tissue: a review from a microscopist's perspective. *J. Biomed. Opt.* **21**, 081205 (2016).
77. Glaser, A. K. et al. Multi-immersion open-top light-sheet microscope for high-throughput imaging of cleared tissues. *Nat. Commun.* **10**, 2781 (2019).
78. Elfer, K. N. et al. DRAQ5 and eosin ('D&E') as an analog to hematoxylin and eosin for rapid fluorescence histology of fresh tissues. *PLoS ONE* **11**, e0165530 (2016).
79. Mao, C. et al. Feature-rich covalent stains for super-resolution and cleared tissue fluorescence microscopy. *Sci. Adv.* **6**, eaba4542 (2020).
80. Chowdary, D. et al. Prognostic gene expression signatures can be measured in tissues collected in RNAlater preservative. *J. Mol. Diagn.* **8**, 31–39 (2006).
81. Mutter, G. L. et al. Comparison of frozen and RNALater solid tissue storage methods for use in RNA expression microarrays. *BMC Genomics* **5**, 88 (2004).

82. Ergin, B. et al. Proteomic analysis of PAXgene-fixed tissues. *J. Proteome Res.* **9**, 5188–5196 (2010).
83. Urban, C. et al. PAXgene fixation enables comprehensive metabolomic and proteomic analyses of tissue specimens by MALDI MSI. *Biochim. Biophys. Acta* **1862**, 51–60 (2018).
84. Park, Y.-G. et al. Protection of tissue physicochemical properties using polyfunctional crosslinkers. *Nat. Biotechnol.* **37**, 73–83 (2018).
85. González-García, I., Solé, R. V. & Costa, J. Metapopulation dynamics and spatial heterogeneity in cancer. *Proc. Natl Acad. Sci. USA* **99**, 13085–13089 (2002).
86. Chung, K. & Deisseroth, K. CLARITY for mapping the nervous system. *Nat. Methods* **10**, 508–513 (2013).
87. Susaki, E. A. et al. Advanced CUBIC protocols for whole-brain and whole-body clearing and imaging. *Nat. Protoc.* **10**, 1709–1727 (2015).
88. Tainaka, K. et al. Whole-body imaging with single-cell resolution by tissue decolorization. *Cell* **159**, 911–924 (2014).
89. Yoshitake, T. et al. Direct comparison between confocal and multiphoton microscopy for rapid histopathological evaluation of unfixed human breast tissue. *J. Biomed. Opt.* **21**, 126021 (2016).
90. Tu, H. et al. Stain-free histopathology by programmable supercontinuum pulses. *Nat. Photon.* **10**, 534–540 (2016).
91. Helmchen, F. & Denk, W. Deep tissue two-photon microscopy. *Nat. Methods* **2**, 932–940 (2005).
92. Uhlén, P. & Tanaka, N. Improved pathological examination of tumors with 3D light-sheet microscopy. *Trends Cancer* **4**, 337–341 (2018).
93. Pouli, D. et al. Imaging mitochondrial dynamics in human skin reveals depth-dependent hypoxia and malignant potential for diagnosis. *Sci. Transl. Med.* **8**, 367ra169 (2016).
94. Baugh, L. M. et al. Non-destructive two-photon excited fluorescence imaging identifies early nodules in calcific aortic-valve disease. *Nat. Biomed. Eng.* **1**, 914–924 (2017).
95. Skala, M. C. et al. In vivo multiphoton microscopy of NADH and FAD redox states, fluorescence lifetimes, and cellular morphology in precancerous epithelia. *Proc. Natl Acad. Sci. USA* **104**, 19494–19499 (2007).
96. You, S. et al. Label-free visualization and characterization of extracellular vesicles in breast cancer. *Proc. Natl Acad. Sci. USA* **116**, 24012–24018 (2019).
97. Xylas, J., Alt-Holland, A., Garlick, J., Hunter, M. & Georgakoudi, I. Intrinsic optical biomarkers associated with the invasive potential of tumor cells in engineered tissue models. *Biomed. Opt. Express* **1**, 1387–1400 (2010).
98. Conklin, M. W. et al. Aligned collagen is a prognostic signature for survival in human breast carcinoma. *Am. J. Pathol.* **178**, 1221–1232 (2011).
99. Campagnola, P. J. & Loew, L. M. Second-harmonic imaging microscopy for visualizing biomolecular arrays in cells, tissues and organisms. *Nat. Biotechnol.* **21**, 1356–1360 (2003).
100. Freudiger, C. W. et al. Label-free biomedical imaging with high sensitivity by stimulated Raman scattering microscopy. *Science* **322**, 1857–1861 (2008).
101. Saar, B. G. et al. Video-rate molecular imaging in vivo with stimulated Raman scattering. *Science* **330**, 1368–1370 (2010).
102. Fischer, M. C., Wilson, J. W., Robles, F. E. & Warren, W. S. Invited review article: pump-probe microscopy. *Rev. Sci. Instrum.* **87**, 031101 (2016).
103. Matthews, T. E., Piletic, I. R., Selim, M. A., Simpson, M. J. & Warren, W. S. Pump-probe imaging differentiates melanoma from melanocytic nevi. *Sci. Transl. Med* **3**, 71ra15 (2011).
104. Giacomelli, M. G. et al. Multiscale nonlinear microscopy and widefield white light imaging enables rapid histological imaging of surgical specimen margins. *Biomed. Opt. Express* **9**, 2457–2475 (2018).
105. Nakano, A. Spinning-disk confocal microscopy—a cutting-edge tool for imaging of membrane traffic. *Cell Struct. Funct.* **27**, 349–355 (2002).
106. Tanaami, T. et al. High-speed 1-frame/ms scanning confocal microscope with a microlens and Nipkow disks. *Appl. Opt.* **41**, 4704–4708 (2002).
107. Cheng, L.-C. et al. Spatiotemporal focusing-based widefield multiphoton microscopy for fast optical sectioning. *Opt. Express* **20**, 8939–8948 (2012).
108. Oron, D., Tal, E. & Silberberg, Y. Scanningless depth-resolved microscopy. *Opt. Express* **13**, 1468–1476 (2005).
109. Zhang, T. et al. Kilohertz two-photon brain imaging in awake mice. *Nat. Methods* **16**, 1119–1122 (2019).
110. Bewersdorf, J., Pick, R. & Hell, S. W. Multifocal multiphoton microscopy. *Opt. Lett.* **23**, 655–657 (1998).
111. Bahlmann, K. et al. Multifocal multiphoton microscopy (MMM) at a frame rate beyond 600 Hz. *Opt. Express* **15**, 10991–10998 (2007).
112. Dodt, H.-U. et al. Ultramicroscopy: three-dimensional visualization of neuronal networks in the whole mouse brain. *Nat. Methods* **4**, 331–336 (2007).
113. Fahrbach, F. O., Simon, P. & Rohrbach, A. Microscopy with self-reconstructing beams. *Nat. Photon.* **4**, 780–785 (2010).
114. Huisken, J., Swoger, J., Del Bene, F., Wittbrodt, J. & Stelzer, E. H. K. Optical sectioning deep inside live embryos by selective plane illumination microscopy. *Science* **305**, 1007–1009 (2004).
115. Keller, P. J. et al. Fast, high-contrast imaging of animal development with scanned light sheet-based structured-illumination microscopy. *Nat. Methods* **7**, 637–642 (2010).
116. Keller, P. J., Schmidt, A. D., Wittbrodt, J. & Stelzer, E. H. K. Reconstruction of zebrafish early embryonic development by scanned light sheet microscopy. *Science* **322**, 1065–1069 (2008).
117. Planchon, T. A. et al. Rapid three-dimensional isotropic imaging of living cells using Bessel beam plane illumination. *Nat. Methods* **8**, 417–423 (2011).
118. Power, R. M. & Huisken, J. A guide to light-sheet fluorescence microscopy for multiscale imaging. *Nat. Methods* **14**, 360–373 (2017).
119. Tomer, R. et al. SPED light sheet microscopy: fast mapping of biological system structure and function. *Cell* **163**, 1796–1806 (2015).
120. Wu, Y. et al. Spatially isotropic four-dimensional imaging with dual-view plane illumination microscopy. *Nat. Biotechnol.* **31**, 1032–1038 (2013).
121. Scherf, N. & Huisken, J. The smart and gentle microscope. *Nat. Biotechnol.* **33**, 815–818 (2015).
122. Fahrbach, F. O., Gurchenkov, V., Alessandri, K., Nassoy, P. & Rohrbach, A. Light-sheet microscopy in thick media using scanned Bessel beams and two-photon fluorescence excitation. *Opt. Express* **21**, 13824–13839 (2013).
123. Tomer, R., Ye, L., Hsueh, B. & Deisseroth, K. Advanced CLARITY for rapid and high-resolution imaging of intact tissues. *Nat. Protoc.* **9**, 1682–1697 (2014).
124. Marx, V. Microscopy: seeing through tissue. *Nat. Methods* **11**, 1209–1214 (2014).
125. Wu, Y. et al. Inverted selective plane illumination microscopy (iSPIM) enables coupled cell identity lineaging and neurodevelopmental imaging in *Caenorhabditis elegans*. *Proc. Natl Acad. Sci. USA* **108**, 17708–17713 (2011).
126. Migliori, B. et al. Light sheet theta microscopy for rapid high-resolution imaging of large biological samples. *BMC Biol.* **16**, 57–19 (2018).
127. Mcgorty, R. et al. Open-top selective plane illumination microscope for conventionally mounted specimens. *Opt. Express* **23**, 16142–16153 (2015).
128. Voigt, F. F. et al. The mesoSPIM initiative: open-source light-sheet microscopes for imaging cleared tissue. *Nat. Methods* **16**, 1105–1108 (2019).
129. Chakraborty, T. et al. Light-sheet microscopy of cleared tissues with isotropic, subcellular resolution. *Nat. Methods* **16**, 1109–1113 (2019).
130. Bouchard, M. B. et al. Swept confocally-aligned planar excitation (SCAPE) microscopy for high speed volumetric imaging of behaving organisms. *Nat. Photon.* **9**, 113–119 (2015).
131. Voleti, V. et al. Real-time volumetric microscopy of in vivo dynamics and large-scale samples with SCAPE 2.0. *Nat. Methods* **16**, 1054–1062 (2019).
132. Yang, B. et al. Epi-illumination SPIM for volumetric imaging with high spatial-temporal resolution. *Nat. Methods* **16**, 501–504 (2019).
133. Strnad, P. et al. Inverted light-sheet microscope for imaging mouse pre-implantation development. *Nat. Methods* **13**, 139–142 (2016).
134. Barner, L. A., Glaser, A. K., True, L. D., Reder, N. P. & Liu, J. T. C. Solid immersion meniscus lens (SIMlens) for open-top light-sheet microscopy. *Opt. Lett.* **44**, 4451–4454 (2019).
135. Dunsby, C. Optically sectioned imaging by oblique plane microscopy. *Opt. Express* **16**, 20306–20316 (2008).
136. Millett-Sikking, A. & York, A. AndrewGYork/high_na_single_objective_lightsheet: work-in-progress. Zenodo https://doi.org/10.5281/zenodo.3376243 (2019).
137. Kumar, M., Kishore, S., Nasenbeny, J., McLean, D. L. & Kozorovitskiy, Y. Integrated one- and two-photon scanned oblique plane illumination (SOPi) microscopy for rapid volumetric imaging. *Opt. Express* **26**, 13027–13041 (2018).
138. Sapoznik, E. et al. A versatile oblique plane microscope for large-scale and high-resolution imaging of subcellular dynamics. *eLife* **9**, 279 (2020).
139. Bishop, K. W., Glaser, A. K. & Liu, J. T. C. Performance tradeoffs for single- and dual-objective open-top light-sheet microscope designs: a simulation-based analysis. *Biomed. Opt. Express* **11**, 4627–4650 (2020).
140. Glaser, A. K., Bishop, K. W., Barner, L. A., Serafin, R. B. & Liu, J. T. C. A hybrid open-top light-sheet microscope for multi-scale imaging of cleared tissues. Preprint at *bioRxiv* https://doi.org/10.1101/2020.05.06.081745 (2020).
141. Barner, L. A., Glaser, A. K., Huang, H., True, L. D. & Liu, J. T. C. Multi-resolution open-top light-sheet microscopy to enable efficient 3D pathology workflows. *Biomed. Opt. Express* **11**, 6605–6619 (2020).
142. Bria, A., Bernaschi, M., Guarrasi, M. & Iannello, G. Exploiting multi-level parallelism for stitching very large microscopy images. *Front. Neuroinform.* **13**, 41 (2019).
143. Bria, A. & Iannello, G. TeraStitcher—a tool for fast automatic 3D-stitching of teravoxel-sized microscopy images. *BMC Bioinformatics* **13**, 316 (2012).
144. Hörl, D. et al. BigStitcher: reconstructing high-resolution image datasets of cleared and expanded samples. *Nat. Methods* **16**, 870–874 (2019).
145. Amat, F. et al. Efficient processing and analysis of large-scale light-sheet microscopy data. *Nat. Protoc.* **10**, 1679–1696 (2015).
146. Balazs, B., Deschamps, J., Albert, M., Ries, J. & Hufnagel, L. A real-time compression library for microscopy images. Preprint at *bioRxiv* https://doi.org/10.1101/164624 (2017).

147. Stefansson, H. N. et al. Wavelet compression of three-dimensional time-lapse biological image data. *Microsc. Microanal.* **11**, 9–17 (2005).
148. Giacomelli, M. G. et al. Virtual hematoxylin and eosin transillumination microscopy using epi-fluorescence imaging. *PLoS ONE* **11**, e0159337 (2016).
149. Serafin, R., Xie, W., Glaser, A. K. & Liu, J. T. C. FalseColor-Python: a rapid intensity-leveling and digital-staining package for fluorescence-based slide-free digital pathology. *PLoS ONE* **15**, e0233198 (2020).
150. Schindelin, J. et al. Fiji: an open-source platform for biological-image analysis. *Nat. Methods* **9**, 676–682 (2012).
151. Schneider, C. A., Rasband, W. S. & Eliceiri, K. W. NIH Image to ImageJ: 25 years of image analysis. *Nat. Methods* **9**, 671–675 (2012).
152. Rueden, C. T. et al. ImageJ2: ImageJ for the next generation of scientific image data. *BMC Bioinformatics* **18**, 529 (2017).
153. Edelstein, A., Amodaj, N., Hoover, K., Vale, R. & Stuurman, N. Computer control of microscopes using manager. *Curr. Protoc. Mol. Biol.* **92**, 14.20.1–14.20.17 (2010).
154. Pietzsch, T., Saalfeld, S., Preibisch, S. & Tomancak, P. BigDataViewer: visualization and processing for large image data sets. *Nat. Methods* **12**, 481–483 (2015).
155. Pitrone, P. G. et al. OpenSPIM: an open-access light-sheet microscopy platform. *Nat. Methods* **10**, 598–599 (2013).
156. Marx, V. Microscopy: OpenSPIM 2.0. *Nat. Methods* **13**, 979–982 (2016).
157. Carpenter, A. E., Kamentsky, L. & Eliceiri, K. W. A call for bioimaging software usability. *Nat. Methods* **9**, 666–670 (2012).
158. Cardona, A. & Tomancak, P. Current challenges in open-source bioimage informatics. *Nat. Methods* **9**, 661–665 (2012).
159. Ghaznavi, F., Evans, A., Madabhushi, A. & Feldman, M. Digital imaging in pathology: whole-slide imaging and beyond. *Annu. Rev. Pathol.* **8**, 331–359 (2013).
160. Niazi, M. K. K., Parwani, A. V. & Gurcan, M. N. Digital pathology and artificial intelligence. *Lancet Oncol.* **20**, e253–e261 (2019).
161. Pantanowitz, L. et al. Review of the current state of whole slide imaging in pathology. *J. Pathol. Inform.* **2**, 36 (2011).
162. Vaidya, P. et al. CT derived radiomic score for predicting the added benefit of adjuvant chemotherapy following surgery in stage I, II resectable non-small cell lung cancer: a retrospective multi-cohort study for outcome prediction. *Lancet Digit. Health* **2**, e116–e128 (2020).
163. Madabhushi, A. & Lee, G. Image analysis and machine learning in digital pathology: challenges and opportunities. *Med. Image Anal.* **33**, 170–175 (2016).
164. Cheplygina, V., de Bruijne, M. & Pluim, J. P. W. Not-so-supervised: a survey of semi-supervised, multi-instance, and transfer learning in medical image analysis. *Med. Image Anal.* **54**, 280–296 (2019).
165. Tajbakhsh, N., Jeyaseelan, L., Li, Q., Chiang, J. N., Wu, Z. & Ding, X. Embracing imperfect datasets: A review of deep learning solutions for medical image segmentation. *Med. Image Anal.* **63**, 101693 (2020).
166. He, K., Fan, H., Wu, Y., Xie, S. & Girshick, R. Momentum contrast for unsupervised visual representation learning. Preprint at https://arxiv.org/abs/1911.05722 (2019).
167. Khan, A. M., Rajpoot, N., Treanor, D. & Magee, D. A nonlinear mapping approach to stain normalization in digital histopathology images using image-specific color deconvolution. *IEEE Trans. Biomed. Eng.* **61**, 1729–1738 (2014).
168. Belthangady, C. & Royer, L. A. Applications, promises, and pitfalls of deep learning for fluorescence image reconstruction. *Nat. Methods* **16**, 1215–1225 (2019).
169. Bhargava, H. K. et al. Computationally derived image signature of stromal morphology is prognostic of prostate cancer recurrence following prostatectomy in African American patients. *Clin. Cancer Res.* **26**, https://doi.org/10.1158/1078-0432.CCR-19-2659 (2020).
170. Chandramouli, S. et al. Computer extracted features from initial H&E tissue biopsies predict disease progression for prostate cancer patients on active surveillance. *Cancers* **12**, 2708 (2020).
171. Christiansen, E. M. et al. In silico labeling: predicting fluorescent labels in unlabeled images. *Cell* **173**, 792–803 (2018).
172. Ounkomol, C., Seshamani, S., Maleckar, M. M., Collman, F. & Johnson, G. R. Label-free prediction of three-dimensional fluorescence images from transmitted-light microscopy. *Nat. Methods* **15**, 917–920 (2018).
173. Kiemen, A. et al. In situ characterization of the 3D microanatomy of the pancreas and pancreatic cancer at single cell resolution. Preprint at *bioRxiv* https://doi.org/10.1101/2020.12.08.416909 (2020).
174. Maier, A. K. et al. Learning with known operators reduces maximum training error bounds. *Nat. Mach. Intell.* **1**, 373–380 (2019).
175. Maier, A., Syben, C., Lasser, T. & Riess, C. A gentle introduction to deep learning in medical image processing. *Z. Med. Phys.* **29**, 86–101 (2019).
176. Dou, Q. et al. 3D deeply supervised network for automated segmentation of volumetric medical images. *Med. Image Anal.* **41**, 40–54 (2017).
177. Martel, A. L. et al. An image analysis resource for cancer research: PIIP—Pathology Image Informatics Platform for visualization, analysis, and management. *Cancer Res.* **77**, e83–e86 (2017).
178. Bankhead, P. et al. QuPath: open source software for digital pathology image analysis. *Sci. Rep.* **7**, 16878 (2017).
179. Rivenson, Y. et al. Virtual histological staining of unlabelled tissue-autofluorescence images via deep learning. *Nat. Biomed. Eng.* **3**, 466–477 (2019).
180. Jackson, C. R., Sriharan, A. & Vaickus, L. J. A machine learning algorithm for simulating immunohistochemistry: development of SOX10 virtual IHC and evaluation on primarily melanocytic neoplasms. *Mod. Pathol.* **33**, 1638–1648 (2020).
181. Janowczyk, A., Zuo, R., Gilmore, H., Feldman, M. & Madabhushi, A. HistoQC: an open-source quality control tool for digital pathology slides. *JCO Clin. Cancer Inform.* https://doi.org/10.1200/CCI.18.00157 (2019).
182. Leo, P. et al. Stable and discriminating features are predictive of cancer presence and Gleason grade in radical prostatectomy specimens: a multi-site study. *Sci. Rep.* **8**, 14918 (2018).
183. Liu, J. et al. An integrated TCGA Pan-Cancer Clinical Data Resource to drive high-quality survival outcome analytics. *Cell* **173**, 400–416 (2018).
184. Paik, S. et al. Gene expression and benefit of chemotherapy in women with node-negative, estrogen receptor-positive breast cancer. *J. Clin. Oncol.* **24**, 3726–3734 (2006).
185. Paik, S. et al. A multigene assay to predict recurrence of tamoxifen-treated, node-negative breast cancer. *N. Engl. J. Med* **351**, 2817–2826 (2004).
186. Bast, R. C. & Hortobagyi, G. N. Individualized care for patients with cancer—a work in progress. *N. Engl. J. Med.* **351**, 2865–2867 (2004).
187. Engel, K. B., Vaught, J. & Moore, H. M. National Cancer Institute biospecimen evidence-based practices: a novel approach to pre-analytical standardization. *Biopreserv. Biobank.* **12**, 148–150 (2014).
188. Sparano, J. A. et al. Prospective validation of a 21-gene expression assay in breast cancer. *N. Engl. J. Med.* **373**, 2005–2014 (2015).
189. Allen, T. C. Food and Drug Administration approval of laboratory tests. *Arch. Pathol. Lab. Med.* **137**, 13–18 (2013).
190. Evans, A. J. et al. US Food and Drug Administration approval of whole slide imaging for primary diagnosis: a key milestone is reached and new questions are raised. *Arch. Pathol. Lab. Med.* **142**, 1383–1387 (2018).
191. Mukhopadhyay, S. et al. Whole slide imaging versus microscopy for primary diagnosis in surgical pathology: a multicenter blinded randomized noninferiority study of 1992 cases (pivotal study). *Am. J. Surg. Pathol.* **42**, 39–52 (2018).
192. Joly, Y. et al. Regulatory approval for new pharmacogenomic tests: a comparative overview. *Food Drug Law J.* **66**, 1–24 (2011).
193. D'Angelo, R. et al. Facing the inevitable: being prepared for regulatory requirements for laboratory developed tests. *Am. J. Clin. Pathol.* **149**, 484–498 (2018).
194. Madabhushi, A., Feldman, M. D. & Leo, P. Deep-learning approaches for Gleason grading of prostate biopsies. *Lancet Oncol.* **21**, 187–189 (2020).
195. King, C. R. & Long, J. P. Prostate biopsy grading errors: a sampling problem? *Int J. Cancer* **90**, 326–330 (2000).
196. Ruijter, E., van Leenders, G., Miller, G., Debruyne, F. & van de Kaa, C. Errors in histological grading by prostatic needle biopsy specimens: frequency and predisposing factors. *J. Pathol.* **192**, 229–233 (2000).
197. Campanella, G. et al. Clinical-grade computational pathology using weakly supervised deep learning on whole slide images. *Nat. Med.* **25**, 1301–1309 (2019).
198. Chen, D. S. & Mellman, I. Elements of cancer immunity and the cancer-immune set point. *Nature* **541**, 321–330 (2017).
199. Rizvi, N. A. et al. Mutational landscape determines sensitivity to PD-1 blockade in non-small cell lung cancer. *Science* **348**, 124–128 (2015).
200. Viaud, S. et al. The intestinal microbiota modulates the anticancer immune effects of cyclophosphamide. *Science* **342**, 971–976 (2013).
201. Vétizou, M. et al. Anticancer immunotherapy by CTLA-4 blockade relies on the gut microbiota. *Science* **350**, 1079–1084 (2015).
202. Herbst, R. S. et al. Predictive correlates of response to the anti-PD-L1 antibody MPDL3280A in cancer patients. *Nature* **515**, 563–567 (2014).
203. Gajewski, T. F., Schreiber, H. & Fu, Y.-X. Innate and adaptive immune cells in the tumor microenvironment. *Nat. Immunol.* **14**, 1014–1022 (2013).
204. Corredor, G. et al. Spatial architecture and arrangement of tumor-infiltrating lymphocytes for predicting likelihood of recurrence in early-stage non-small cell lung cancer. *Clin. Cancer Res.* **25**, 1526–1534 (2019).
205. Annecchino, L. A. et al. Robotic automation of in vivo two-photon targeted whole-cell patch-clamp electrophysiology. *Neuron* **95**, 1048–1055 (2017).
206. Long, B., Li, L., Knoblich, U., Zeng, H. & Peng, H. 3D image-guided automatic pipette positioning for single cell experiments in vivo. *Sci. Rep.* **5**, 18426 (2015).
207. Suk, H.-J. et al. Closed-loop real-time imaging enables fully automated cell-targeted patch-clamp neural recording in vivo. *Neuron* **95**, 1037–1047 (2017).

208. Li, L. et al. Co-registration of ex vivo surgical histopathology and in vivo T2 weighted MRI of the prostate via multi-scale spectral embedding representation. *Sci. Rep.* **7**, 8717 (2017).
209. Rusu, M. et al. Co-registration of pre-operative CT with ex vivo surgically excised ground glass nodules to define spatial extent of invasive adenocarcinoma on in vivo imaging: a proof-of-concept study. *Eur. Radiol.* **27**, 4209–4217 (2017).
210. Rusu, M. et al. Prostatome: a combined anatomical and disease based MRI atlas of the prostate. *Med. Phys.* **41**, 072301 (2014).
211. Antunes, J. et al. Coregistration of preoperative MRI with ex vivo mesorectal pathology specimens to spatially map post-treatment changes in rectal cancer onto in vivo imaging: preliminary findings. *Acad. Radiol.* **25**, 833–841 (2018).
212. Schillaci, O. et al. Combining diagnostic imaging and pathology for improving diagnosis and prognosis of cancer. *Contrast Media Mol. Imaging* **2019**, 9429761 (2019).
213. Grönroos, T. J. et al. Hypoxia, blood flow and metabolism in squamous-cell carcinoma of the head and neck: correlations between multiple immunohistochemical parameters and PET. *BMC Cancer* **14**, 876 (2014).
214. Surov, A., Meyer, H. J. & Wienke, A. Standardized uptake values derived from ^{18}F-FDG PET may predict lung cancer microvessel density and expression of KI 67, VEGF, and HIF-1α but not expression of cyclin D1, PCNA, EGFR, PD L1, and p53. *Contrast Media Mol. Imaging* **2018**, 9257929 (2018).
215. Bensch, F. et al. ^{89}Zr-atezolizumab imaging as a non-invasive approach to assess clinical response to PD-L1 blockade in cancer. *Nat. Med.* **24**, 1852–1858 (2018).
216. Gibson, E. et al. Registration of prostate histology images to ex vivo MR images via strand-shaped fiducials. *J. Magn. Reson. Imaging* **36**, 1402–1412 (2012).
217. Mori, K. From macro-scale to micro-scale computational anatomy: a perspective on the next 20 years. *Med. Image Anal.* **33**, 159–164 (2016).
218. O'Keefe, E. B., Meltzer, J. P. & Bethea,T. N. Health disparities and cancer: racial disparities in cancer mortality in the United States, 2000–2010. *Front. Public Health* **3**, 51 (2015).
219. Zhou, M. et al. Non-small cell lung cancer radiogenomics map identifies relationships between molecular and imaging phenotypes with prognostic implications. *Radiology* **286**, 307–315 (2018).
220. Vaidya, P. et al. RaPtomics: integrating radiomic and pathomic features for predicting recurrence in early stage lung cancer. In *Proc. SPIE 10581, Medical Imaging 2018: Digital Pathology* (eds Gurcan, M. N. & Tomaszewski, J. E.) 105810M (International Society for Optics and Photonics, 2018).
221. Savage, R. S. & Yuan, Y. Predicting chemoinsensitivity in breast cancer with 'omics/digital pathology data fusion. *R. Soc. Open Sci.* **3**, 140501 (2016).
222. Pinker, K., Chin, J., Melsaether, A. N., Morris, E. A. & Moy, L. Precision medicine and radiogenomics in breast cancer: new approaches toward diagnosis and treatment. *Radiology* **287**, 732–747 (2018).
223. Mobadersany, P. et al. Predicting cancer outcomes from histology and genomics using convolutional networks. *Proc. Natl Acad. Sci. USA* **115**, E2970–E2979 (2018).
224. Penzias, G. et al. Identifying the morphologic basis for radiomic features in distinguishing different Gleason grades of prostate cancer on MRI: preliminary findings. *PLoS ONE* **13**, e0200730 (2018).
225. Dainis, A. M. & Ashley, E. A. Cardiovascular precision medicine in the genomics era. *JACC Basic Transl. Sci.* **3**, 313–326 (2018).
226. Kai, C., Uchiyama, Y., Shiraishi, J., Fujita, H. & Doi, K. Computer-aided diagnosis with radiogenomics: analysis of the relationship between genotype and morphological changes of the brain magnetic resonance images. *Radiol. Phys. Technol.* **11**, 265–273 (2018).
227. Montalto, M. C. An industry perspective: an update on the adoption of whole slide imaging. *J. Pathol. Inform.* **7**, 18 (2016).

Acknowledgements

We acknowledge research grants from the Department of Defense (DoD) Prostate Cancer Research Program through W81XWH-18-10358 (J.T.C.L. and L.D.T.), W81XWH-19-1-0589 (N.P.R.), W81XWH-20-1-0851(A.M. and J.T.C.L.) and W81XWH-15-1-0558 (A.M.); the DoD Breast Cancer Research Program W81XWH-19-1-0668 (A.M.); the DoD Lung Cancer Research Program W81XWH-18-1-0440 (A.M.); the DoD Peer Reviewed Cancer Research Program W81XWH-16-1-0329 (A.M.); the Ohio Third Frontier Technology Validation Fund (A.M.); the Wallace H. Coulter Foundation Program in the Department of Biomedical Engineering and The Clinical and Translational Science Award Program at Case Western Reserve University (A.M.); the Prostate Cancer Foundation (N.P.R.); and the National Science Foundation 1934292 HDR: I-DIRSE-FW (J.T.C.L.). We also acknowledge grants from the National Institutes of Health (NIH) National Cancer Institute (NCI) through K99CA240681 (A.K.G.), R01CA175391 (J.T.C.L.), R01CA244170 (J.T.C.L.), R01CA199996 (K.W.E.), U24CA199374 (A.M.), R01CA202752 (A.M.), R01CA208236 (A.M.), R01CA216579 (A.M.), R01CA220581 (A.M.), R01CA249992 (A.M.), U01CA248226 (A.M.), U54CA254566 (A.M.) and U01CA239055 (A.M.); from the NIH National Institute of Biomedical Imaging and Bioengineering (NIBIB) through R43EB028736 (A.M.); from the NIH National Heart, Lung and Blood Institute (NHLBI) through R01HL151277 (A.M.); from the NIH National Institute of General Medical Sciences (NIGMS) through P41GM135019 (K.W.E.); from the NIH National Center for Research Resources through C06RR12463 (A.M.); from the US Department of Veterans Affairs IBX004121A (A.M.); from the Institute for Prostate Cancer Research at the University of Washington (L.D.T.), and from the National Cancer Institute Breast Cancer SPORE/Safeway Foundation at the Fred Hutchinson Cancer Research Center (J.T.C.L). The content is solely the responsibility of the authors and does not necessarily represent the official views of the National Institutes of Health, the US Department of Veterans Affairs, the Department of Defense or the United States Government.

Author contributions

All authors discussed and wrote the manuscript. J.T.C.L. and A.K.G. drew the figures. J.T.C.L. coordinated the effort and led the writing.

Competing interests

J.T.C.L., A.K.G., N.P.R. and L.D.T. are co-founders and shareholders of Lightspeed Microscopy, of which J.T.C.L. and N.P.R. are board members and N.P.R. is the chief executive officer. Technology developed by J.T.C.L., A.K.G., N.P.R. and L.D.T. at the University of Washington has been licensed by Lightspeed Microscopy. K.W.E. is a co-founder and shareholder of OnLume, and a scientific advisory consultant for Bruker Corporation and Elephas Corporation. A.M. is an equity holder in Elucid Bioimaging and Inspirata, has served as a scientific advisory board member for Inspirata, AstraZeneca, Bristol Myers-Squibb, Aiforia and Merck, has had sponsored research agreements with Philips and Inspirata, has technology that is licensed to Elucid Bioimaging and Inspirata, and is involved in a NIH U24 grant with PathCore Inc. and in three different R01 grants with Inspirata Inc. A.M. has sponsored research projects from AstraZeneca, Bristol Myers-Squibb and Boehringer-Ingelheim.

Additional information

Correspondence should be addressed to J.T.C.L., K.W.E. or A.M.